Accepted Manuscript

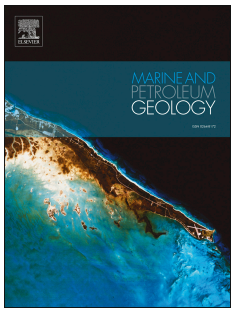

A multidisciplinary approach for sustainable management of a complex coastal plain: The case of Sibari Plain (Southern Italy)

Giovanni Vespasiano, Giuseppe Cianflone, Andrea Romanazzi, Carmine Apollaro, Rocco Dominici, Maurizio Polemio, Rosanna De Rosa

PII: S0264-8172(19)30283-1

DOI: https://doi.org/10.1016/j.marpetgeo.2019.06.031

Reference: JMPG 3892

To appear in: *Marine and Petroleum Geology*

Received Date: 3 January 2019

Revised Date: 7 June 2019

Accepted Date: 17 June 2019

Please cite this article as: Vespasiano, G., Cianflone, G., Romanazzi, A., Apollaro, C., Dominici, R., Polemio, M., De Rosa, R., A multidisciplinary approach for sustainable management of a complex coastal plain: The case of Sibari Plain (Southern Italy), *Marine and Petroleum Geology* (2019), doi: https://doi.org/10.1016/j.marpetgeo.2019.06.031.

A multidisciplinary approach for sustainable management of a complex coastal plain: the case of Sibari Plain (Southern Italy)

Vespasiano Giovanni [1,3 *], Cianflone Giuseppe [1,3 *] ✉, Romanazzi Andrea [2], Apollaro Carmine [1], Dominici Rocco [1,3], Polemio Maurizio [2] & De Rosa Rosanna [1]

[1] Dept. of Biology, Ecology and Earth Sciences (DIBEST), University of Calabria, via Ponte Bucci 4, cubo 15B, I-87036 Arcavacata di Rende (CS), Italy;

[2] CNR-IRPI, National Research Council, Research Institute for Hydrogeological Protection, Via Amendola 122 I, Bari, 70126, Italy

[3] EalCUBO (Earth, Environment, Engineering) Soc. Coop - University of Calabria, via Ponte Bucci, cubo 15B, I-87036 Arcavacata di Rende (CS), Italy.

✉ Corresponding author, e-mail: giuseppe.cianflone@unical.it

*****_These authors have contributed equally to this work._

Keywords: *Sibari Plain; seawater intrusion; Hydro-stratigraphic reconstruction; Hydro-geochemical characterization; hydrogeological modelling.*

Abstract

Coastal plain environments constantly adapt to change as a result of natural processes and increasing anthropogenic pressure, as in the case of the low relief Sibari coastal plain (Calabria, southern Italy).

In order to reconstruct the hydrostratigraphic framework and explain the spatial distribution of groundwater salinization of the Sibari coastal plain, an integrated hydrogeological and geochemical approach was applied to support an accurate conceptualisation and modelling of the whole plain groundwater system. Litho-hydro-stratigraphic relationships were constructed from lithologic logs obtained from exploratory boreholes whereas, the groundwater flow system has been studied using conventional hydrogeological field investigations, hydrochemistry, and isotope hydrology.

Three distinct Hydrological units (HU3-shallow aquifer, HU2 aquitard and HU1-lower aquifer) were identified showing distinct geometrical, hydrochemical and isotopic signatures.

With the aim of explain the origin of Na-Cl, Ca-Cl and Na-HCO_3 waters were considered the role of ion exchange processes. The results demonstrate that values of Na^+, Mg^{2+}, Cl and SO_4 can be attributed to seawater intrusion, where K^+ is probably the major pollutant of the shallow aquifer.

The adopted multidisciplinary approach provides an effective tool for accurately determination of groundwater processes and can be useful for a sustainable management of water resources in coastal plain. The physically based model of the pail groundwater system was able to explain the observed groundwater salinity variations and to support a detailed long-lasting numerical simulation of variations in the quantity and quality of groundwater resources.

1. Introduction

The sustainable development and management of coastal plain has received significant attention worldwide during the last decades (Boughriba and Jilali, 2018; Matiatos et al. 2018). Coastal areas and coastal plains are experiencing the adverse consequences of hazards related to geological processes, climate change and sea-level rise. The impact is exacerbated by increasing human-induced pressure due to land-use and hydrological changes, including reclamation works, embankments, dams and overexploitation of groundwater.

In most of Mediterranean coastal areas, especially in Italy (Polemio and Lonigro, 2015; Polemio, 2016; Sanford et al. 2007), one of the main problem for the governance is the overexploitation of groundwater to meet the growing population demand which increases the effect of salinization processes, subsidence and/or flood damages (Bocanegra et al. 2007; Changming et al. 2001; De Montety et al. 2008; Haruyama 2016). The vulnerability of coastal aquifers to water extraction and land use have been estimated by several studies indicating that their impact is more significant than the impact of sea-level rise. However, the relationship among surface and sea water bodies, groundwater flow, geological features and aquifer features has not been enough scientifically examined for a wide range of coastal plains and coastal aquifers.

This study offers a contribution in this framework, investigating with a multidisciplinary approach a peculiar coastal plain. The approach integrates the study of geological and geochemical data with hydrogeological information and the physical state, including recent modifications, of the coastline. All the data were applied to support an accurate conceptualization and modelling of the whole Sibari plain focusing on geochemical processes and groundwater quality and use.

The attention is focused on the Sibari coastal Plain, located in Calabria Region (Southern Italy), which is very important as an active agricultural and tourist zone (Fig. 1). The Sibari Plain is located on the Ionian coast and represents a large coastal alluvial plain where considerable reclamation works have been able to permit a diffuse agricultural development, based on the use of groundwater, and a relevant urbanization during the latest 60 years (Petrucci and Polemio, 2007). This area is characterized by low rainfall (mean annual value lower than 600 mm) and the decreasing trend of effective rainfall (Cianflone et al. 2015a; Polemio et al. 2004a), related to climate changes effects recorded in southern Italy, which exposes it to increasing dryness risk (Polemio et al. 2004b).

Two well-defined aquifers were recognized in the SPGS by Polemio and Luise, (2007). The shallow aquifer is located at deep up to -30 m asl, and at the bottom, a clayey and silty-clayey layer (aquitard), reaching -50/-60 m asl, divides the shallow aquifer from the deeper one consisting of gravel and sand of upper Pleistocene age (Fig.1).

In the middle of the plain (corresponding to the floodplain of the Crati and Coscile Rivers), groundwater salinization was observed up to about 10 km landward from the coastline (Fig.1) (Casmez, 1987). This salinization was attributed to different causes such us seawater intrusion due to intense groundwater overexploitation, interactions with rocks containing halite and/or upconing of deep saline water (Guerricchio et al. 1976; Guerricchio and Ronconi, 1997; Tazioli, 1986). Guerricchio et al. (1976) showed a strong mineralization of the deep aquifer groundwater with a high content of reduced sulfur species, iron, manganese, carbon dioxide and methane.

The results will provide essential guidelines for an optimum management of groundwater protection and pumping in the study area.

2. Study Area: Geological Setting

The SP is located in correspondence of the boundary between the igneous-metamorphic terranes of the Calabrian Arc and the carbonate units of the Southern Apennines.

The Calabrian Arc is a nappe made by Hercynian and pre-Hercynian continental basement (including metamorphic rocks and their sedimentary covers intruded by igneous batholith) and Jurassic to Early Cretaceous ophiolite-bearing sequences (Amodio Morelli et al., 1976; Messina et al., 1994; Bonardi et al., 2001). Neogene sedimentary basins onlap Ionian and Tyrrhenian sides of the Calabrian Arc inner core.

During Miocene, the Calabrian Arc overthrusted upon the Triassic-Miocene Apennine-Maghrebian chain (Amodio Morelli et alii, 1976; Finetti et alii, 1996). The latter, outcropping along the northwestern side of the SP, consists of Mesozoic-Tertiary carbonatic succession and “flyschoid” deposits of the Saraceno and Albidona Formations (ISPRA, 2009 and references therein). The Saraceno Formaion, consisting of an arenaceous-pelitic alternance with late Jurassic (*Torricelli & Amore*, 2003) or late Eocene-Aquitanian age (*Di Staso & Giardino*, 2002), crops out along the nothwestern side of the SP.The SP is bounded by the Sila Massif southward and the Pollino Massif northward (Fig. 1). From the structural point of view, the plain-massifs boundary is marked by dislocations related to the Pliocene-Holocene high angle faults whose recent activity is still a matter of debate (Cucci, 2004; Ferranti et al. 2009; Lanzafame and Tortorici, 1981; Molin et al. 2004). Lanzafame and Tortorici, (1981) suggest the existence of NE-SW normal faults in the middle of the plain; evidences of a NE-SW fault zone with recent activity have been observed as coseismic features in the *Sybaris* archeological settlement by Cinti et al. (2015) and in geophysical acquisitions by Cianflone et al. (2018).

In the northern sector of the SP, the bedrock is represented by the Saraceno Formation (Selli, 1962). It is overlapped by a Pliocene marly-clayey unit (Torrente Straface Unit; ISPRA, 2009),, passing upward to Pleistocene sandy marine deposits (Caruso et al., 2013) and Holocene coarse-grained alluvial sediments (ISPRA, 2009).

The middle sector of the SPGS is characterized by a thick (up to ~2.5 km) Neogene sedimentary filling, which unconformably overlays the bedrock due to Calabrian and Southern Apennines terranes. The sedimentary succession consists of late Miocene terrigenous and evaporite sediments, which outcrop in the Rossano Basin (Barone et al. 2008; Perri et al. 2015), passing-upward to Pliocene marly-clays (locally confined by the presence of structural highs) overlapped by Quaternary alternation of coarse and fine-grained deposits (Spina et al. 2011). The evaporites of Messinian age include gypsum and halite deposits (the thickness of the halite -bearing beds is greater than 400 m, as in the case of the hydrocarbon exploration well Thurio) related to the Messinian Salinity Crisis (Cianflone et al. 2018; Vespasiano et. al. 2015b).

The main morphological structures clearly represented in the middle sector of investigated area is the double-winged Crati Delta. The present position is the result of delta migration with time starting 2 km eastward from the archeological site of Favella della Corte at the end of the post-glacial sea level rise (5-6 ka B.P.) (Bellotti et al. 2003, 2009). The Holocene evolution is controlled by the post-glacial sea level rise, sediment supply of the Crati River and other streams (e.g., Coscile and Garda Rivers, Raganello and Satanasso Streams) which flowed into the plain, tectonic activity and human-made factors (Bellotti et al. 2003, 2009; Guerricchio and Melidoro, 1975; Pagliarulo, 2006).

In the southern sector of the SP, the bedrock consists of the igneous-metamorphic rocks of the Calabrian Arc overlapped by Miocene arenites and conglomerates and Pliocene clays (Casmez, 1967). The latter pass upward to Pleistocene marine deposits (mainly sand) and alluvial sediments (Casmez, 1967).

Along the plain boundaries, the main morphological elements are represented by alluvial fans (Fig. 2), which are well developed in the northern sector where they are related to the Raganello, Satanasso (active since the middle Pleistocene) and Saraceno (active since ~3 ka B.P.) streams (Guerricchio and Melidoro, 1975; Sabato and Tropeano, 2008).

Various orders of marine terraces are recognized along the outer limit of the SPGS by different authors (7 orders by Cucci and Cinti, 1998; 11 orders by Santoro et al., 2009). It is noteworthy that The SP is characterized by high subsidence rate in historical time with a peak of 5–6 mm/yr in the Early Holocene (Ferranti et al. 2011) and at present up to 20 mm/yr (Cianflone et al. 2015b, 2015c) times.

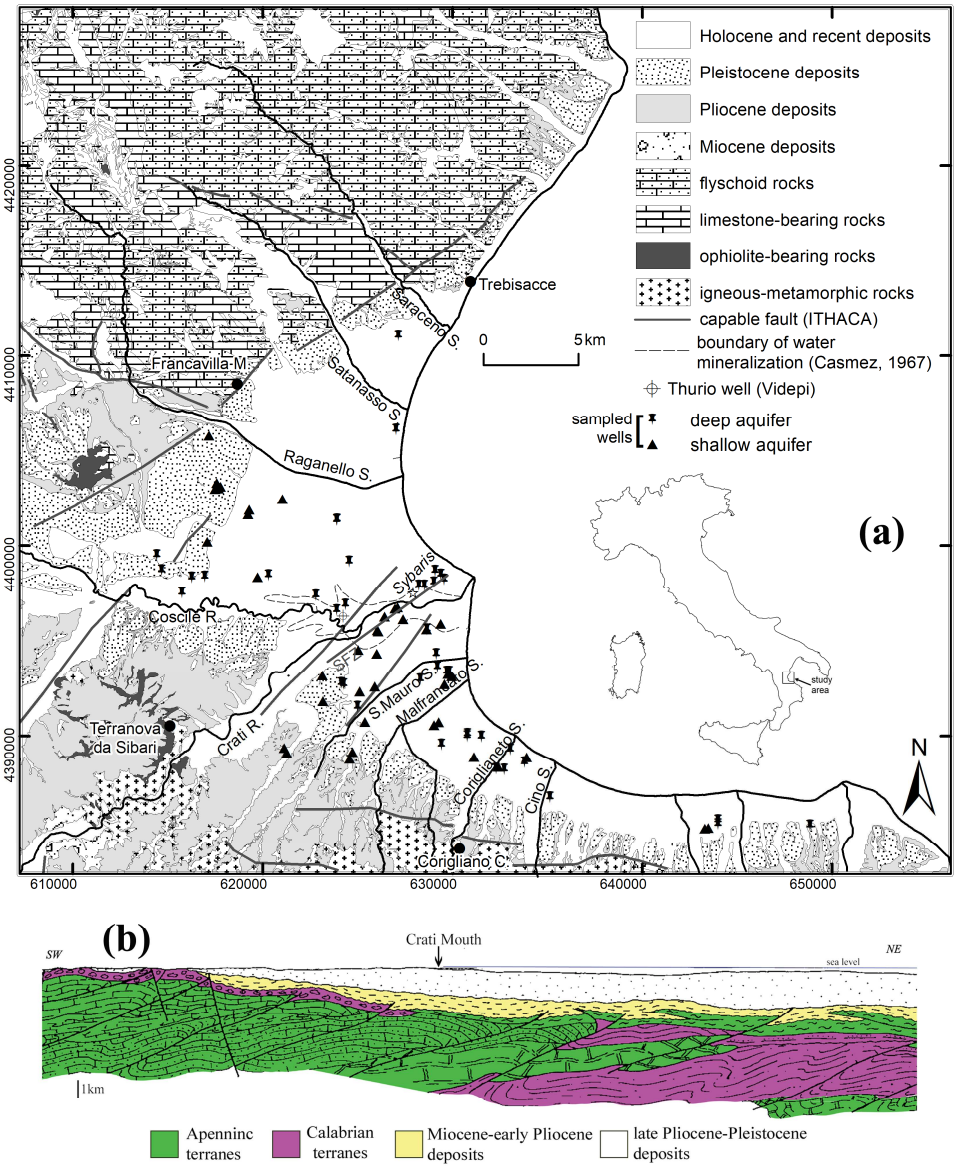

Figure 1 – (a) Simplified geological map of the study area. Fault traces are derived from Ithaca database (Comerci et al., 2013) while Sybaris Fault Zone (SZF) is from Cinti et al. (2015). (b) Deep seismic profile, modified from Cello et al. (1981), showing the thin Calabrid units overlapping the Southern Apennine units.

3. Methodology

a. Site data collection

A three-dimensional facies-belt model based on sedimentological and stratigraphic data is essential to investigate the hydrogeological characteristics of a sedimentary aquifer (Fraser and Davis, 1998). The analysis of hydrostratigraphic framework was based on the integration of sedimentological and stratigraphic data with field survey observation. Boreholes data were acquired from public and private institutions (e.g., Demanio Idrico della Provincia di Cosenza, ANAS S.p.A.), scientific papers (Bernasconi et al. 2010; Casmez, 1987; Cherubini et al. 2000; Guerricchio and Melidoro, 1975; Hofman, 2002; ISPRA, 2009) and the open access database of boring and well data (ISPRA geodatabase). Stratigraphic data were used to create hydro-stratigraphic cross-sections.

Borehole data were integrated by electrical resistivity profiles, where available (Casmez, 1987).

The relative permeability of distinguished strata, assessed mainly on the basis of grain size, was used to recognise hydrogeological complexes and bottom and top surfaces of aquifers.

We investigated the geometry of the SPGS pursuing the detailed three-dimensional knowledge of the aquitard located between shallow and deep aquifers of SPGS. For this purpose, 130 and 74 boreholes were analysed and the Digital Surface Models (DSMs) of the aquitard top and bottom were assessed. (these boreholes are shown in Figure 3). Using DSMs and the DTM (Digital Terrain Model) 20x20 m (GN), we estimate thickness and geometrical features of the aquitard and shallow aquifer. Distribution of drillhole data points was used in hydrostratigraphic surface interpolation.

To improve the knowledge on groundwater chemical composition and on water cycle, a geochemical survey was carried out on 80 selected wells from June to September 2012 (Figure 2). The majority of these wells were drilled by private for withdraw water; for this reason, data on screen depth and stratigraphy are not generally available. Well depth ranges from 5 m to 167 m

(with 60, 50 and 40 m as mean, median and standard deviation respectively) (Table 1a and b). As it is a common constructing practice the screen installation in the whole thickness of the selected aquifer, well depth was compared to the top and bottom of the aquitard (HU2) to define the aquifer tapped by each considered well (DSM). This approach allowed to identify two main groups of wells: shallow (39 wells) and deep (41 wells).

b. Analytical geochemical methods;

The methodology of water sampling and analysis was described by Apollaro et al. 2015, Apollaro et al. 2016; Apollaro et al. 2019; Critelli et al. 2015; Vardè et al. 2018; Vespasiano et al. 2014 and Vespasiano et al. 2015d. Nevertheless, it is reported here below to make this contribution self-consistent.

Prior to sampling, wells were purged either removing three times the volume for each well or until stabilization of field parameters. Water standing in a well for a period of time undergoes changes that can impact several parameters including pH, Eh, alkalinity/acidity, hardness, and the concentration of metals, sulphate, dissolved solids, and dissolved oxygen.

After preliminary purging operation, intrinsically unstable parameters as temperature, pH, Eh, total alkalinity, and electrical conductivity (EC) were measured in the field by means of portable instruments. Two pH buffers, with nominal pH values of 4.01 and 7.01 at 25 °C, were used for pH calibration at each sampling site. Total alkalinity was determined by acidimetric titration, using HCl 0.05N and 0.01N as titrating agent and methylorange as indicator. Water samples were filtered in situ through a membrane with a 0.4 μm pore size to remove suspended solids and colloids. Samples for the determination of anions, $\delta^{18}O$ and $\delta^{2}H$ values were stored without additional treatments, whereas samples for the determination of cations and SiO_2 were acidified after filtration by addition of suprapure acid (1% HNO_3) and stored. All the samples were stored in polyethylene bottles, previously washed in dilute HNO_3 and rinsed with Milli-Q demineralized water. All the water samples were stored at 4 °C in dark conditions before analysis. In the laboratory, the concentrations

194 of F^-, Cl^-, Br^-, SO_4^{2-}, NO_3^-, PO_4^{3-}, Na^+, K^+, Mg^{2+} and Ca^{2+} were determined by HPLC (DIONEX
195 ICS 1100). On the same day that samples were collected, dissolved reactive SiO_2 was measured by
196 VIS spectrophotometry, upon reaction with ammonium molybdate in acid media and treatment with
197 oxalic acid, to form a yellow silicomolybdate complex, whose absorbance was read at 410 nm (see
198 Nollet and De Gelder, 2007 for further details). The $\delta^{18}O$ and $\delta^{2}H$ values of SPGS water samples
199 were measured in the laboratories of the Stable Isotope Unit, Institute of Geosciences and Earth
200 Resources (IGG-CNR, Pisa) on a Finnigan TC/EA stable isotope mass spectrometer.
201 Data quality for major components was estimated by charge balance. Deviation between the sum of
202 concentrations of cations and the sum of concentrations of anions, both in equivalent units, varies
203 between -5% and +5%. The results of laboratory analyses and field data are shown in Table 1a and
204 b.
205 Geochemical data were analyzed following a consolidated procedure which comprises the
206 classification of waters and the inspection of chloride plots. Furthermore, for a better understanding
207 of the ion exchange processes, data were modelled by the EQ3/6 software package (Wolery and
208 Jarek, 2003) adopting the Vanselow convention for the cation exchanger and assuming the presence
209 of a single exchange site (see section 4.3.2).
210

Table 1a. Field parameters and concentrations of major chemical components and selected minor components in the SPGS wells. (d.l. = detection limit; n.d. = not detected; n.a. = not available).

ID	UTM (WGS84)	UTM (WGS84)	pH	Eh	T	EC	Ca	Mg	K	Na	Sr	NH_4	Cl	SO_4	HCO_3	F	NO_3	Br	SiO_2	Depth	Aquifer
	X	Y		mV	°C	mS/cm	ppm	ppm	ppm	ppm	ppm	ppm	ppm	ppm	ppm	ppm	ppm	ppm	ppm	m	
P1	632409	4388390	7.44	275	18.7	0.299	49.26	8.71	0.89	20.80	< d.l.	< d.l.	7.75	13.89	170.85	0.15	3.44	< d.l.	15.50	15	HU3
P2	629268	4390723	7.47	256	18.2	0.842	103.37	29.79	6.02	31.03	< d.l.	< d.l.	65.85	96.22	321.86	0.21	4.53	< d.l.	18.00	12	HU3
P3	629022	4390572	7.37	225	17.9	0.777	104.50	29.95	6.27	33.13	< d.l.	< d.l.	51.93	90.16	318.81	0.15	5.01	< d.l.	18.00	25	HU3
P4	633908	4388896	6.88	260	21.9	0.562	67.22	17.08	2.53	25.94	< d.l.	< d.l.	15.22	77.41	205.93	0.34	14.04	< d.l.	16.75	7	HU3
P5	627109	4396738	7.13	35	18.4	1.175	162.98	42.23	4.72	57.25	< d.l.	< d.l.	73.80	165.78	540.00	0.06	< d.l.	< d.l.	11.00	8	HU3
P6	631125	4388906	7.17	92	19.1	0.793	78.22	19.28	5.16	60.17	< d.l.	< d.l.	66.37	76.28	334.07	0.91	1.13	< d.l.	20.25	22	HU3
P7	626970	4396679	7.22	-18	18.0	0.935	110.39	26.02	7.28	77.77	< d.l.	< d.l.	40.89	99.44	558.31	0.09	0.77	< d.l.	11.50	7	HU3
P8	626421	4396262	7.88	-40	21.9	1.398	114.35	39.94	15.33	129.45	< d.l.	< d.l.	215.68	17.18	466.78	0.22	< d.l.	< d.l.	16.75	11	HU3
P9	626036	4395546	8.02	168	22.1	1.054	104.33	33.63	7.24	81.40	< d.l.	< d.l.	130.32	121.93	355.42	0.23	1.91	< d.l.	12.50	12	HU3
P10	625391	4390734	7.18	108	16.8	0.799	101.95	31.98	4.21	37.21	< d.l.	< d.l.	42.76	93.16	352.37	0.20	3.83	< d.l.	16.50	25	HU3
P11	617074	4400202	7.10	165	18.2	0.819	97.40	40.41	2.53	32.93	< d.l.	< d.l.	49.59	68.64	384.41	0.24	19.03	< d.l.	12.75	25	HU3
P12	643486	4385170	7.05	169	19.1	1.053	161.68	23.83	2.29	35.26	3.92	< d.l.	44.43	54.74	448.47	0.25	65.22	< d.l.	11.00	30	HU3
P13	643291	4385149	6.98	203	19.8	1.014	147.85	19.74	3.80	36.12	3.82	0.56	42.92	61.72	417.97	0.20	71.02	< d.l.	11.90	25	HU3
P14	624731	4389164	7.09	-124	17.8	1.247	127.33	43.26	8.32	83.91	2.38	1.69	81.69	249.63	424.07	0.39	< d.l.	< d.l.	17.30	70	HU3
P15	629583	4392704	7.51	184	n.d.	0.621	52.11	14.38	2.42	56.62	0.72	< d.l.	67.84	52.99	207.46	0.57	8.39	< d.l.	14.70	15	HU3
P16	626015	4394310	7.42	-106	21.0	1.029	92.26	34.19	5.41	77.75	1.60	< d.l.	93.88	67.05	411.86	0.41	0.00	0.34	17.40	22	HU3
P17	625115	4392319	7.13	228	18.3	0.885	103.39	34.69	3.86	41.52	2.13	< d.l.	53.53	101.64	343.22	0.46	18.55	0.81	16.40	40	HU3
P18	629762	4393233	7.51	-69	20.0	1.642	132.94	58.81	1.12	130.00	1.70	1.62	184.09	99.39	605.59	0.60	< d.l.	1.48	18.40	30	HU3
P19	625895	4392581	7.54	-124	18.8	0.788	72.50	26.20	4.23	47.20	1.65	1.15	46.98	38.04	385.93	0.65	0.12	0.19	17.60	35	HU3
P20	623141	4393166	7.73	-193	21.6	0.944	73.89	31.73	7.25	79.37	1.24	1.51	117.09	51.08	346.27	0.19	< d.l.	0.40	16.60	42	HU3
P21	619721	4398347	6.46	-122	20.9	0.630	74.57	33.38	3.65	50.59	1.86	2.61	65.48	9.07	425.59	0.33	< d.l.	0.53	13.20	37	HU3
P22	617173	4405805	6.30	29	20.0	0.812	74.84	35.74	1.66	29.95	1.70	< d.l.	64.44	50.17	361.53	0.12	< d.l.	< d.l.	12.70	35	HU3
P23	621130	4389376	7.54	124	18.1	1.107	108.59	44.03	6.37	65.72	1.95	< d.l.	67.42	167.37	428.64	0.30	2.70	< d.l.	19.00	52	HU3
P24	621265	4389119	7.24	87	16.2	0.881	85.40	32.63	5.04	56.53	1.73	< d.l.	57.14	121.03	353.90	0.56	6.57	0.57	13.90	45	HU3
P25	623172	4391821	7.48	250	23.8	0.675	67.40	24.40	3.17	39.27	1.16	< d.l.	39.27	79.58	268.47	0.49	9.16	< d.l.	14.00	38	HU3
P26	621037	4402457	7.11	119	18.3	1.038	125.84	45.11	2.10	27.39	2.57	< d.l.	27.46	202.75	411.86	0.11	37.82	< d.l.	4.60	40	HU3
P27	617770	4403117	7.29	191	19.8	1.390	113.50	35.95	4.14	86.39	1.97	< d.l.	150.53	119.13	407.29	0.26	24.68	0.44	10.20	50	HU3
P28	617493	4402992	7.21	206	22.9	0.900	75.68	23.09	4.58	81.93	1.32	1.18	81.28	34.67	424.07	0.25	2.20	< d.l.	9.00	30	HU3
P29	617581	4403317	7.13	185	20.1	0.945	88.84	23.36	3.94	64.21	1.50	0.92	57.65	56.09	416.44	0.25	22.86	< d.l.	10.30	25	HU3
P30	619283	4401902	8.21	150	20.0	0.600	78.40	19.38	2.03	24.44	1.31	0.35	15.63	96.35	259.32	0.25	6.09	< d.l.	3.10	60	HU3
P31	619230	4401659	7.70	201	23.2	1.403	164.42	65.79	2.60	55.34	3.59	< d.l.	79.27	238.93	491.19	0.21	49.99	< d.l.	5.00	15	HU3
P32	629374	4395881	7.67	104	19.7	1.529	61.55	39.02	23.55	240.23	< d.l.	< d.l.	144.36	78.24	626.95	0.57	< d.l.	< d.l.	13.00	5	HU3
P33	627396	4396117	7.46	-112	17.3	1.397	104.10	36.32	18.41	142.77	< d.l.	< d.l.	247.42	1.40	562.88	0.13	< d.l.	< d.l.	16.25	18	HU3
P34	626079	4395481	7.65	185	24.0	1.991	73.66	87.94	19.82	256.89	< d.l.	< d.l.	316.97	175.83	651.36	1.23	45.94	< d.l.	14.00	12	HU3
P35	625038	4394495	7.74	6	23.0	1.723	126.53	54.77	17.30	192.57	< d.l.	< d.l.	237.07	90.34	695.59	0.09	1.90	< d.l.	15.75	12	HU3
P36	624577	4388815	7.82	-271	21.8	1.695	72.88	46.04	19.00	223.46	1.21	6.99	250.82	170.46	529.32	0.40	< d.l.	0.85	23.60	20	HU3
P37	629960	4393115	7.66	-65	22.9	0.696	50.52	16.15	4.88	70.89	0.52	1.51	97.62	< d.l.	265.42	0.44	< d.l.	0.26	15.70	50	HU3
P38	628632	4395592	7.50	-110	19.1	1.886	90.26	41.99	28.08	258.95	< d.l.	< d.l.	408.64	< d.l.	511.02	0.11	< d.l.	< d.l.	16.50	13	HU3
P39	617667	4403032	7.24	226	20.0	2.030	185.94	58.37	2.99	142.30	3.55	< d.l.	384.13	233.19	276.10	0.00	154.00	1.06	8.20	50	HU3

Table 1b. Field parameters and concentrations of major chemical components and selected minor components in the SPGS wells (d.l. = detection limit; n.d. = not detected; n.a. = not available).

ID	M (WGS	M (WGS	pH	Eh	T	EC	Ca	Mg	K	Na	Sr	NH_4	Cl	SO_4	HCO_3	F	NO_3	Br	SiO_2	Depth	Aquifer
	X	Y		mV	°C	mS/cm	ppm	ppm	ppm	ppm	ppm	ppm	ppm	ppm	ppm	ppm	ppm	ppm	ppm	m	
P40	624560	4399150	7.48	-71	20.1	0.703	84.84	30.69	4.66	33.36	< d.l.	< d.l.	26.72	71.02	329.49	0.19	< d.l.	< d.l.	15.00	80	HU1
P41	630781	4389990	7.33	-61	18.6	0.672	65.54	14.55	2.84	38.82	< d.l.	< d.l.	64.78	< d.l.	241.02	0.45	< d.l.	< d.l.	25.50	40	HU1
P42	630790	4390095	7.60	-5	18.4	0.491	43.78	11.46	4.96	49.52	< d.l.	< d.l.	56.02	22.16	183.05	0.39	< d.l.	< d.l.	19.75	94	HU1
P43	632303	4388276	7.50	274	22.7	0.516	57.93	17.52	4.62	32.44	< d.l.	< d.l.	43.45	50.65	192.20	0.23	11.31	< d.l.	18.75	67	HU1
P44	629401	4398471	7.77	-23	18.9	0.902	81.71	32.05	11.68	64.58	< d.l.	< d.l.	111.93	< d.l.	395.09	0.16	< d.l.	< d.l.	15.75	100	HU1
P45	629090	4398662	7.74	-41	20.0	0.842	74.68	32.15	3.08	59.37	< d.l.	< d.l.	94.67	< d.l.	315.76	0.20	< d.l.	< d.l.	15.75	120	HU1
P46	627029	4406109	7.35	-86	21.0	1.119	128.72	37.57	6.61	82.05	< d.l.	< d.l.	125.03	163.57	340.17	0.73	< d.l.	< d.l.	17.75	120	HU1
P47	635137	4386770	7.08	236	16.1	0.296	35.72	7.53	2.39	13.47	< d.l.	< d.l.	11.57	44.97	97.63	0.35	11.65	< d.l.	13.50	36	HU1
P48	628310	4392941	7.51	41	18.2	0.607	61.55	8.02	4.36	39.78	< d.l.	< d.l.	56.22	11.82	253.22	0.33	< d.l.	< d.l.	17.50	60	HU1
P49	633795	4388624	7.43	132	16.5	0.551	61.13	17.87	4.35	32.77	< d.l.	< d.l.	45.32	32.16	288.31	0.27	5.74	< d.l.	18.00	100	HU1
P50	632739	4388239	7.25	124	17.8	0.771	96.13	20.87	3.58	42.48	< d.l.	< d.l.	44.11	60.25	324.92	0.37	34.40	< d.l.	18.50	80	HU1
P51	633057	4389284	7.77	-116	16.9	0.447	52.25	13.43	3.62	28.71	< d.l.	< d.l.	36.88	20.56	234.92	0.42	< d.l.	< d.l.	14.00	100	HU1
P52	614423	4399484	7.42	36	18.1	0.799	96.56	43.10	1.13	28.39	< d.l.	< d.l.	36.22	81.26	369.15	0.28	17.18	< d.l.	12.50	95	HU1
P53	614686	4398693	7.48	91	18.2	0.833	100.20	47.93	2.55	31.18	< d.l.	< d.l.	35.25	93.41	396.61	0.26	9.33	< d.l.	15.50	65	HU1
P54	627160	4411061	7.03	180	20.0	0.978	120.61	40.30	5.40	54.09	< d.l.	< d.l.	29.05	161.64	421.02	0.05	17.46	< d.l.	10.25	80	HU1
P55	644002	4385571	7.07	148	20.6	0.752	111.71	17.95	3.89	24.91	5.61	0.36	26.77	81.86	335.59	0.26	19.82	< d.l.	8.80	50	HU1
P56	644001	4385377	7.24	159	20.4	0.746	109.01	18.18	3.94	25.25	5.99	0.38	25.69	88.68	314.24	0.18	16.05	< d.l.	7.90	50	HU1
P57	629208	4393587	7.74	180	22.9	0.507	53.84	14.40	2.70	32.22	0.85	< d.l.	37.36	13.30	227.29	0.43	< d.l.	< d.l.	14.10	80	HU1
P58	624998	4391515	7.73	148	17.6	0.752	82.39	27.87	5.84	38.96	1.61	< d.l.	43.97	87.44	298.98	0.38	3.90	0.15	19.50	80	HU1
P59	615743	4397508	6.03	90	18.8	0.821	82.91	38.55	2.40	32.76	1.95	0.44	47.50	73.61	396.61	0.31	0.78	0.69	13.70	40	HU1
P60	616950	4398364	6.35	-69	19.1	0.814	82.41	34.96	2.72	42.50	2.17	< d.l.	59.07	50.14	392.03	0.48	< d.l.	0.75	16.80	45	HU1
P61	620304	4398438	6.51	-42	19.9	0.777	65.59	28.19	3.40	44.70	1.59	1.87	54.79	0.63	413.39	0.35	< d.l.	0.18	13.60	54	HU1
P62	616266	4398309	7.64	121	18.6	0.901	101.87	38.98	2.54	37.88	2.66	< d.l.	50.12	84.53	404.24	0.54	24.09	< d.l.	9.30	80	HU1
P63	623904	4401329	8.16	168	18.7	0.843	89.50	29.88	3.05	52.73	2.29	< d.l.	66.04	107.01	331.02	0.46	3.23	0.73	10.20	80	HU1
P64	623925	4401357	8.39	156	20.7	0.855	82.48	30.10	3.05	53.68	2.14	< d.l.	68.02	108.07	332.54	0.37	2.32	0.71	10.40	80	HU1
P65	631525	4389955	7.90	-35	17.5	0.520	45.05	13.91	4.77	52.81	< d.l.	< d.l.	63.79	1.31	218.14	0.30	< d.l.	< d.l.	24.75	93	HU1
P66	629148	4394279	7.74	-42	19.2	0.718	59.87	20.55	6.21	71.13	< d.l.	< d.l.	100.20	< d.l.	314.24	0.17	< d.l.	< d.l.	16.00	100	HU1
P67	629721	4393341	7.50	-102	19.4	1.091	51.80	32.53	23.90	116.11	0.95	9.24	102.56	< d.l.	494.24	0.49	< d.l.	0.51	21.00	94	HU1
P68	629840	4393347	7.71	20	22.4	0.848	58.75	19.24	5.85	93.51	0.63	2.06	149.04	< d.l.	309.66	0.41	1.58	0.45	15.40	100	HU1
P69	629022	4398057	7.39	-122	20.4	2.710	85.01	34.56	46.06	406.54	< d.l.	< d.l.	715.79	< d.l.	466.78	0.00	< d.l.	< d.l.	20.00	n.a.	HU1
P70	628527	4397890	7.03	-144	22.4	4.250	115.26	57.94	65.61	631.40	< d.l.	< d.l.	1199.99	< d.l.	324.92	0.00	< d.l.	< d.l.	18.00	n.a.	HU1
P71	622803	4397362	7.46	-68	20.0	1.669	106.27	44.81	18.65	185.47	< d.l.	< d.l.	380.23	1.45	356.95	0.24	< d.l.	< d.l.	17.75	50	HU1
P72	628229	4397892	7.65	155	22.1	2.680	88.32	65.62	47.52	414.51	< d.l.	< d.l.	579.80	30.80	721.53	0.00	< d.l.	< d.l.	17.75	60	HU1
P73	629555	4398207	7.35	-131	19.5	1.382	90.28	40.20	12.74	161.36	< d.l.	< d.l.	285.05	< d.l.	454.58	0.10	< d.l.	< d.l.	16.25	100	HU1
P74	628662	4395574	7.79	-179	18.5	1.545	14.50	13.32	36.22	286.40	< d.l.	< d.l.	309.74	< d.l.	451.53	0.33	< d.l.	< d.l.	21.25	107	HU1
P75	648845	4385294	7.50	35	21.0	3.970	141.88	70.99	42.80	557.53	< d.l.	< d.l.	1069.64	146.72	541.53	0.00	< d.l.	< d.l.	12.25	40	HU1
P76	629418	4389554	7.41	-16	19.1	1.175	101.48	25.52	8.75	116.80	< d.l.	< d.l.	199.45	90.90	309.66	0.17	7.94	< d.l.	15.75	60	HU1
P77	624366	4396884	7.24	-125	19.6	3.950	161.85	81.20	24.00	466.02	3.41	14.41	1154.87	< d.l.	578.14	0.27	< d.l.	4.18	14.30	120	HU1
P78	624275	4392685	8.56	45	20.0	1.086	75.27	29.37	7.99	102.83	1.18	2.49	214.02	16.28	314.24	0.23	< d.l.	0.81	15.70	135	HU1
P79	624145	4392752	7.58	-131	20.4	1.777	120.04	48.87	8.67	145.24	2.53	3.28	517.48	5.62	308.14	0.22	< d.l.	1.90	16.30	99	HU1
P80	623910	4396594	7.44	-80	22.6	1.577	132.69	48.28	15.94	118.61	< d.l.	< d.l.	310.43	< d.l.	472.88	0.14	< d.l.	< d.l.	24.50	150	HU1

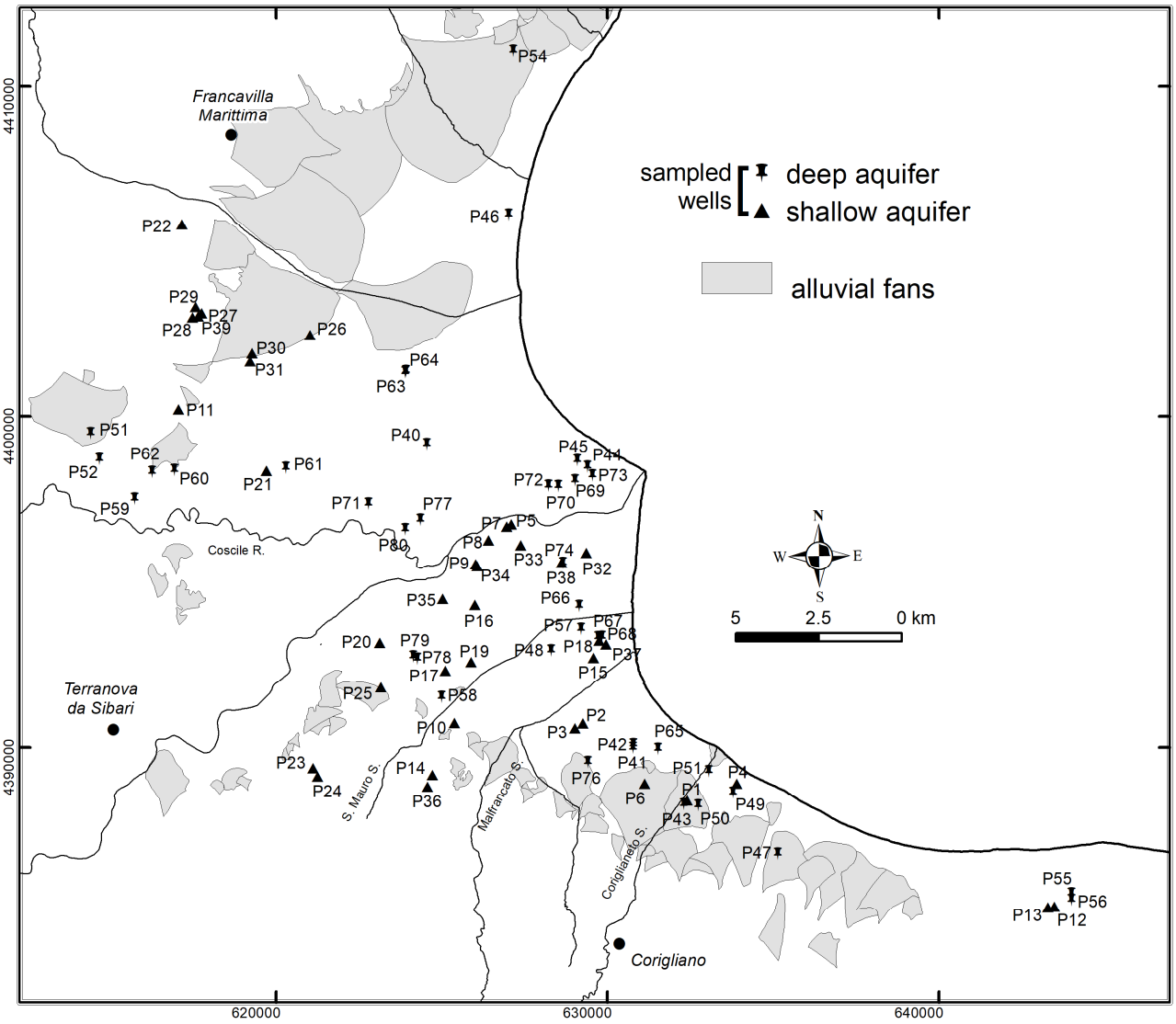

Figure 2 – Location of alluvial fans and sampled wells.

4. Results and Discussion

4.1 Reconstruction of the hydrostratigraphic framework

The stratigraphic framework of the Sibari Plain, related to the post-glacial delta plain evolution and the tectonic setting, represents the key factor to understand the plain hydrogeological features.

In the northernmost sector of the studied area, the hydrostratigraphic framework is controlled by the alluvial fan of the Saraceno stream (Figure 3), which extends from the stream *knick point* to the coastline. The beginning of the alluvial fan aggrading stage occurred 6.5 ka B.P., while the still-active entrenching stage started at 3 ka B.P. (Sabato and Tropeano, 2008). The alluvial fan is mainly made by gravelly deposits, with different textures due to various sedimentological processes (debris flow, sheet flood, stream flood). Sandy bar deposits are less common and the fine-grained overbank sediments are little widespread. The maximum observed thickness of the fan is about 60 m. The coarse-grained deposits overlay, along an erosive surface, the Torrente Straface Marly-Clay unit (ISPRA, 2009), which outcrops a few hundred meters northward and southward from the alluvial fan (Caruso et al. 2013; ISPRA, 2009). The clayey unit lies on top of the Saraceno Formation (Selli, 1962), which is made of an arenaceous-pelitic alternation of controversial origin and age (Bonardi et al. 1988; Caruso et al. 2011; Vezzani, 1968; D'Alessandro et al. 1986; De Blasio et al. 1978; Di Staso and Giardino, 2002; Sonnino, 1984; Torricelli and Amore, 2003).

Southward, the Satanasso stream alluvial fan (Figure 3) represents the main hydrostratigraphic unit. Currently it is not active and is located 2 km landward from the coastline. The fan is made of gravelly deposits with different textures. The estimated thickness reaches about 100 m, but the available data do not allow to define exactly its bottom surface.

Moving southward, the Raganello stream alluvial fan (Figure 3) is the following hydrostratigraphic unit. It consists of a telescopic alluvial fan complex and represents the bigger fan of the SPGS (Guericchio and Melidoro, 1975). The fan thickness observed in the electrical resistivity profile (Casmez, 1987) exceeds 100 m. Boreholes data show 5/10 m-thick silty-sandy deposits on top of the gravelly sediments, which constitute the fan body.

The hydrostratigraphic unit made by the alluvial fan deposits, characterized by complex lateral variations, can be related to a “jigsaw-puzzle” style of facies (Galloway and Sharp, 1998a, 1998b). Instead, in the areas between the alluvial fans a “labyrinth” style of facies (Galloway and Sharp, 1998a, 1998b) is represented by the fine-grained overbank sediments with isolated lens shaped crevasse deposits.

The hydrostratigraphy of the middle sector of the investigated area is strictly related to the Crati Delta stratigraphic framework (Figure 3). In this area, the shallow aquifer consists of the sediments produced by the delta progradation which began about 6 ka B.P. (Bellotti et al. 2009; Cianflone et al. 2018). The underlying aquitard is made of fine-grained deposits related to the post-glacial fast sea-level rise and lies on top of the deep aquifer, which consists of late Pleistocene alluvial plain deposits. The hydrostratigraphic framework is very complicated due to the heteropical transition among the sediments of the different associated depositional environments moving seaward during the delta progradation (Bernasconi et al. 2010; Stanley and Bernasconi, 2009). Another complication of the stratigraphic pattern is due to the repeated captures and separations which characterized the evolution of Crati and Coscile Rivers. Furthermore, the presence of a fault zone with subsurface evidences (Cianflone et al. 2018; Cinti et al., 2015) can represents a potential interchange way between shallow and deep aquifers.

The complex vertical and lateral variations between fine and coarse sediments described above result in a “jigsaw puzzle” style of facies (Galloway and Sharp, 1998a, 1998b).

In the southwestern sector of the Crati River valley, landward from its confluence with the Coscile River (figure 3), the shallow aquifer roughly corresponds to the alluvial deposits, which locally overlay the Pliocene clays (Casmez, 1967). The resistivity profile (Casmez, 1987), located near Terranova da Sibari village, shows a later extension of the alluvial deposits of ~1 km and a maximum thickness of ~75 m, while the profile 6 km towards NE reveals a thickness reaching a maximum value of ~60 m. The boreholes data allow to observe a thickness up to ~250 m for the clays acting as aquitard.

The southernmost area (Figure 3), between S. Mauro and Cino streams, is characterized by telescopic alluvial fan complexes, which started their development in the middle Pleistocene (Guerricchio and Melidoro, 1975).

Based on their main hydrogeological features, each recognized hydrostratigraphic units is converted into an hydrogeological unit (HU), defined as a geologically homogeneous unit (but not necessarily isotropic) that has characteristic hydrodynamic properties (Anderson and Woessner 1992; Sanz et al., 2009). In detail, we identify three main HU:

- HU1 “deep aquifer”, limited to the middle sector and the coastal area, consisting of the coarse-grained deposits of late Pleistocene age;
- HU2 “aquitard”, made up of the Torrente Straface Marly-Clay (northern sector), the Quaternary fine-grained sediments deposited during the post-glacial sea-level rise (middle sector) and the Pliocene clays (southern sector);
- HU3 “shallow aquifer” including the alluvial fans and alluvial plain sediments (northern and southern sectors) and deltaic deposits (middle sector). The coarse grained deposits of river beadload are considered as a subunit (HU3b) of HU3.

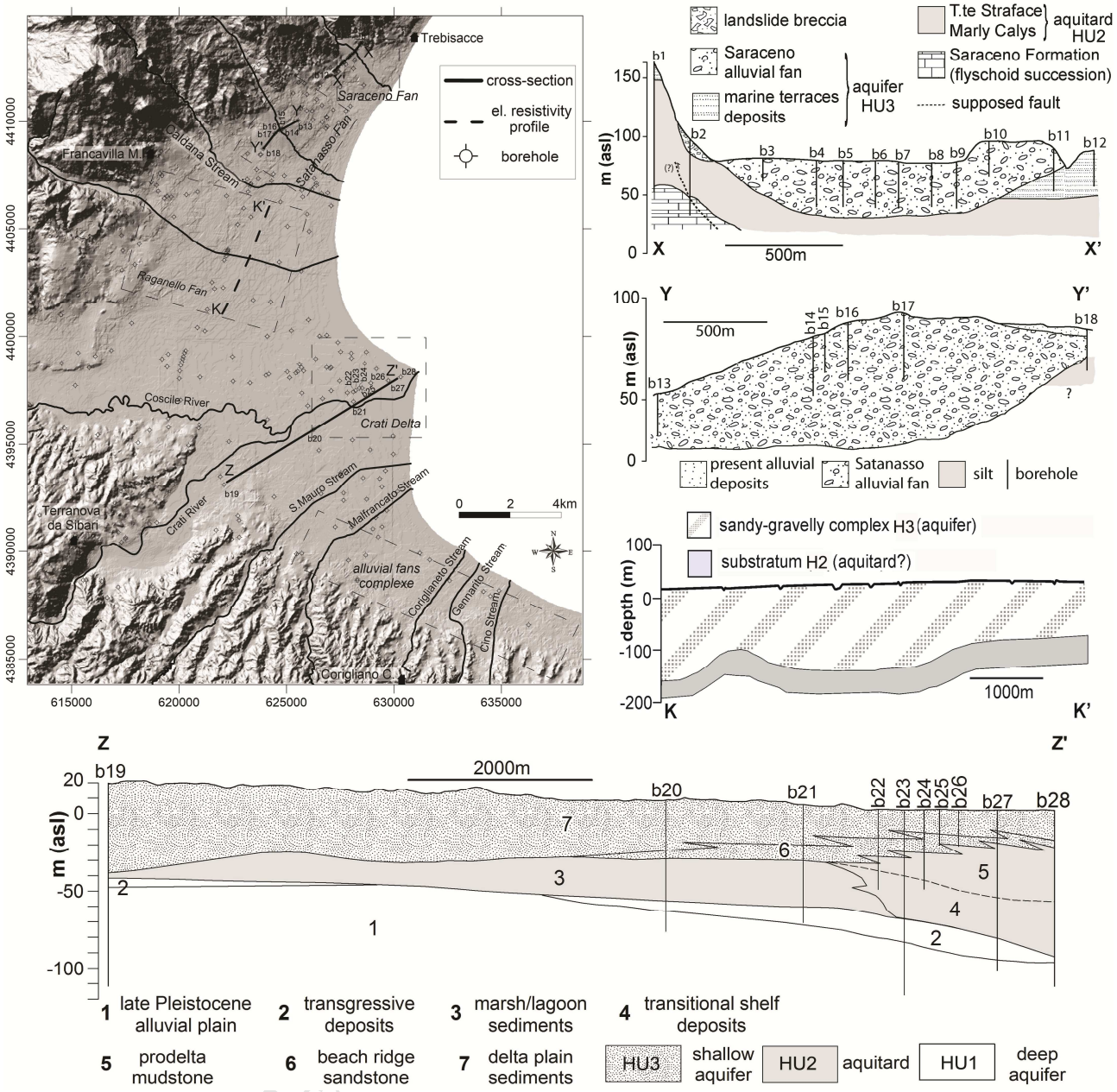

Figure 3 - Hydrostratigraphic cross-sections of the Saraceno alluvial fan (X-X'), the Satanasso alluvial fan (Y-Y') and the Crati Delta area (Z-Z') the electrical resistivity profile crossing the Raganello alluvial fan (K-K', redrawn from Camez, 1987).

The SPGS geometry was analysed starting from DSM of top and bottom of the HU2. The HU3 is characterized by a thickness increasing from W to E and reaching its highest value (~40 m) in the Crati Delta area. In the northernmost sector, near Trebisacce village, the HU3 extension coincides with the coastal area westward bounded by the Pollino Massif. Southward, the HU3 extension increases reaching its maximum in correspondence of the Coscile River Valley. Towards the

southern sector, the extension decreases again due to the presence of the highs bounding the Sila Massif. The DSM of HU2 top intersects the topography in the southwestern sector of the investigated area. In this area, both the evidence acquired during the field survey and the official geological maps (Casmez, 1967) confirm that the HU3 (constituted by clayey deposits with Pliocene age) outcrops (Figure 4).

The depth of the HU2 bottom increases gradually seaward, with the exception of the sector of the Crati Valley close to Terranova da Sibari village. Here, the aquitard bottom reaches ~ -150 m asl and the clayey deposits are 250 m thick.

The HU2 has a wedge shape with thickness increasing seaward, except in the north-western sector. Furthermore, the HU2 thickness decreases up to be negligible in the Raganello alluvial fan, permitting the direct contact between HU1 and HU3. In this area, as shown by the field survey, coarse-grained coastal-deltaic deposits overlap the Lauropoli Conglomerates (Ghisetti and Vezzani, 1983) and springs are present.

Along the SPGS perimeter, the HU2 is due to clayey deposits of Pliocene age, which can be correlated to the Torrente Straface Marly-Clay unit (ISPRA, 2009). Close to the coastline, it is formed by silty-clayey sediments deposited during the last post-glacial transgression (Bellotti et al., 2003; Cianflone et al., 2018).

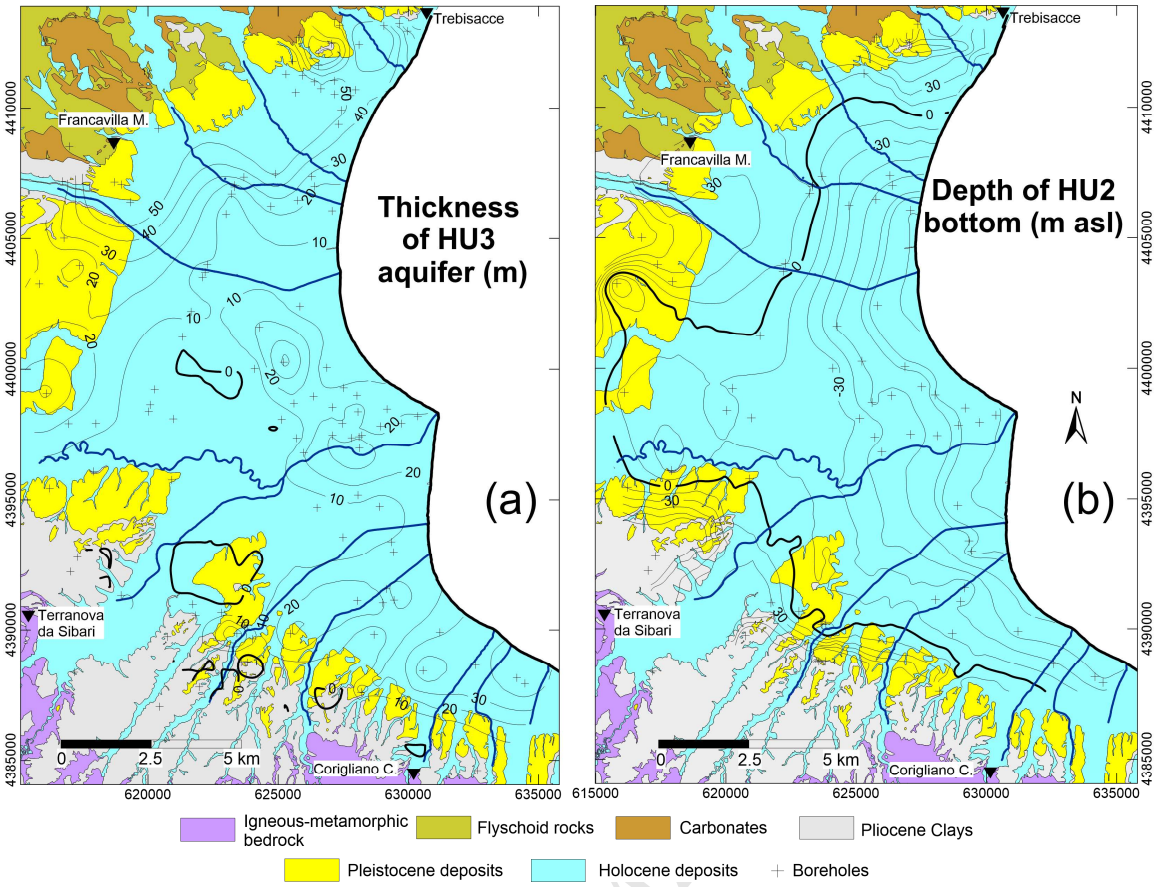

Figure 4 - a) Shallow aquifer HU3 thickness map (m). b) Depth (m asl) of the HU2 aquitard bottom.

4.2 Major hydrochemical aquifers properties

4.2.1 Waters classification

Statistical indices of Eh, temperature (T), pH and electric conductivity (EC) of shallow and deep aquifers of SPGS (HU3 and HU1 hereinafter) are reported in Table 2.

Table 2. Statistical indices of pH, temperature (T), and electric conductivity (EC), and Eh of SPGS groundwaters.

SSPGS aquifer (HU3)	pH	T (°C)	EC (mS/cm) at 25 °C.	Eh (V)
Minimum	6.30	16.20	0.30	-0.27
Maximum	8.21	24.00	2.03	0.28
Average	7.36	19.97	1.08	0.08
Median	7.42	19.80	0.95	0.12

Standard deviation	0.38	2.05	0.42	0.15
DSPGS aquifer (HU1)				
Minimum	6.03	16.10	0.30	-0.18
Maximum	8.56	22.90	4.25	0.27
Average	7.46	19.58	1.20	0.02
Median	7.48	19.50	0.84	0.00
Standard deviation	0.46	1.69	0.96	0.12

A preliminary analysis of these parameters indicates comparable values range for the aquifers considered. In detail:

(i) All wells highlight low discharge temperature with maximum values detected for the shallow aquifer.

(ii) Both the SSPGS and DSPGS aquifers show similar pH and Eh range values. In particular, pH is almost neutral; only five samples have slightly acidic pH (P59, P60 and P61 from the HU1; P21 and P22 from the HU3) and only eight samples have pH values greater than 8 (P9 and P30 from the HU3 and P63, P64 and P78 from HU1.

(iii) EC values highlight the highest variabilities. HU3 Groundwater ranges from 0.30 mS/cm (P1) to 2.03 mS/cm (P39) whereas HU1 ranges from 0.30 (P47) to 4.25 mS/cm (P70).

Temperature, EC, Eh and pH show a wide range of values, suggesting they are due to overlapped effects of more complex phenomena.

The triangular plot of major anions (Figure 5a) shows that HCO_3 prevails in 56 of the 80 samples, followed by Cl that is the predominant anion in 12 samples. The triangular plot of major cations (Figure 5b) shows that Ca prevails in 58 samples, Na is the predominant cation in 22 samples, whereas Mg waters are absent. the Na/K ratio (in equivalent units) varies between 8.2 and 197 and, consequently, Na prevails largely over K.

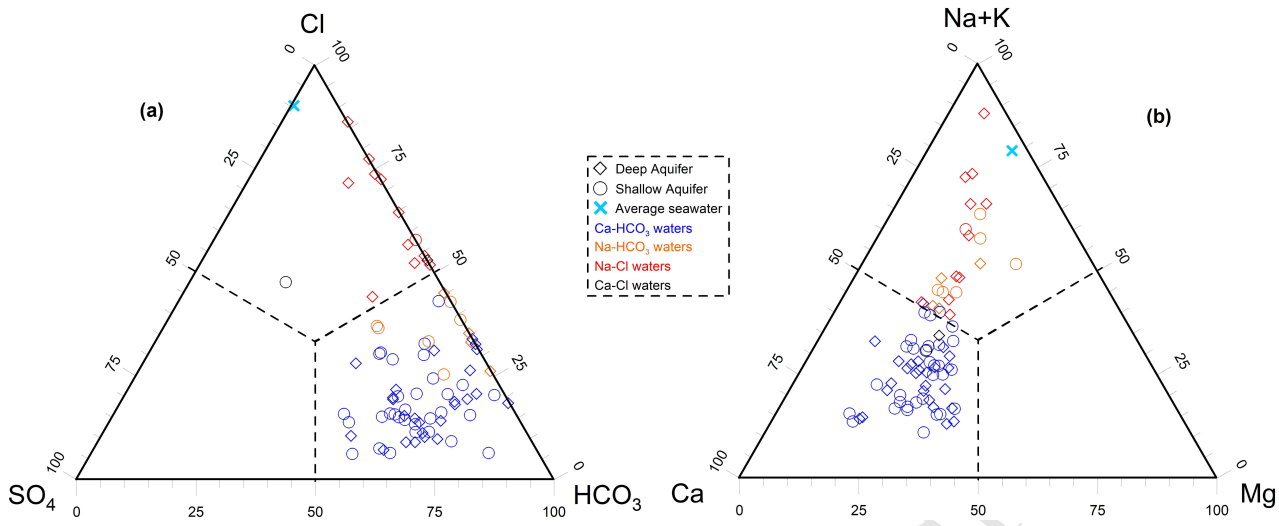

Figure 5. Triangular plots of (a) major anions and (b) major cations for the SPGS groundwaters.

Merging the inferences drawn from the triangular plots of major anions and cations, it can be concluded that the SPGS groundwaters belong to four chemical types:

- $Ca\text{-}HCO_3$, represented by 56 samples, 31 from the HU3 aquifer and 25 from the deep aquifer (HU1);

- $Na\text{-}HCO_3$, comprising 10 samples, 6 from the HU3 aquifer and 4 from the HU1 aquifer;

- Na-Cl, including 12 samples, 1 from the HU3 aquifer and 11 from the HU1 aquifer;

- Ca-Cl, represented by 2 samples only, 1 from the HU3 aquifer and 1 from the HU1 aquifer.

To be noted that:

(i) 80% of the HU3 aquifer samples have $Ca\text{-}HCO_3$ composition, 15% belong to the $Na\text{-}HCO_3$ chemical facies, 2.5% have Na-Cl chemistry, and 2.5% pertain to the Ca-Cl chemical type.

(ii) 61% of the HU1 aquifer samples have $Ca\text{-}HCO_3$ composition, 10% belong to the $Na\text{-}HCO_3$ chemical facies, 27% have Na-Cl chemistry, and 2% pertain to the Ca-Cl chemical type.

Since the $Ca\text{-}HCO_3$ chemical facies is considered representative of freshwaters, whereas the Na-Cl, Ca-Cl and the $Na\text{-}HCO_3$ chemical types are related to seawater intrusion, seawater intrusion accompanied by ion exchange, and freshening respectively, it is evident that HU1 is more influenced by seawater-related processes in respect to HU3. This should be due the natural protection of HU3, the bottom of which is widespread above sea level and, where it is below, as

very close to the sea, it is protected by the aquitard, the bottom of which is many meters below sea level.

As the HU1 top is below sea level, the main protection from salinization due seawater intrusion is to the amount of groundwater flow and of potentiometric level; as they decrease, as effects of withdraws or recharge decreases, seawater intrusion moves inland and upward.

Table 3. The distribution of chemical type in the HU3 and HU1 aquifers

HU3						**HU1**				
Ca-HCO_3			**Na-HCO_3**	**Na-Cl**	**Ca-Cl**	**Ca-HCO_3**		**Na-HCO_3**	**Na-Cl**	**Ca-Cl**
P1	P14	P27	P32	P38	P39	P40	P52	P65	P69	P80
P2	P15	P28	P33			P41	P53	P66	P70	
P3	P16	P29	P34			P42	P54	P67	P71	
P4	P17	P30	P35			P43	P55	P68	P72	
P5	P18	P31	P36			P44	P56		P73	
P6	P19		P37			P45	P57		P74	
P7	P20					P46	P58		P75	
P8	P21					P47	P59		P76	
P9	P22					P48	P60		P77	
P10	P23					P49	P61		P78	
P11	P24					P50	P62		P79	
P12	P25					P51	P63			
P13	P26						P64			

Since the triangular plots of major anions and cations do not deliver any information on the Total Ionic Salinity[1], it is advisable to inspect the correlation plot of $Ca+Mg+HCO_3+SO_4$ vs. $Na+K+Cl$ (Figure 6). In fact, the TIS of water samples can be appreciated in this diagram, by comparing their position with respect to the lines of slope -1 which are iso-TIS lines (Tonani et al. 1998). Figure 6 shows that the four chemical types previously identified have different TIS values.

[1] Total Ionic Salinity is the sum of the concentrations of major cations and anions, all in equivalent units, and is indicated by the acronym TIS.

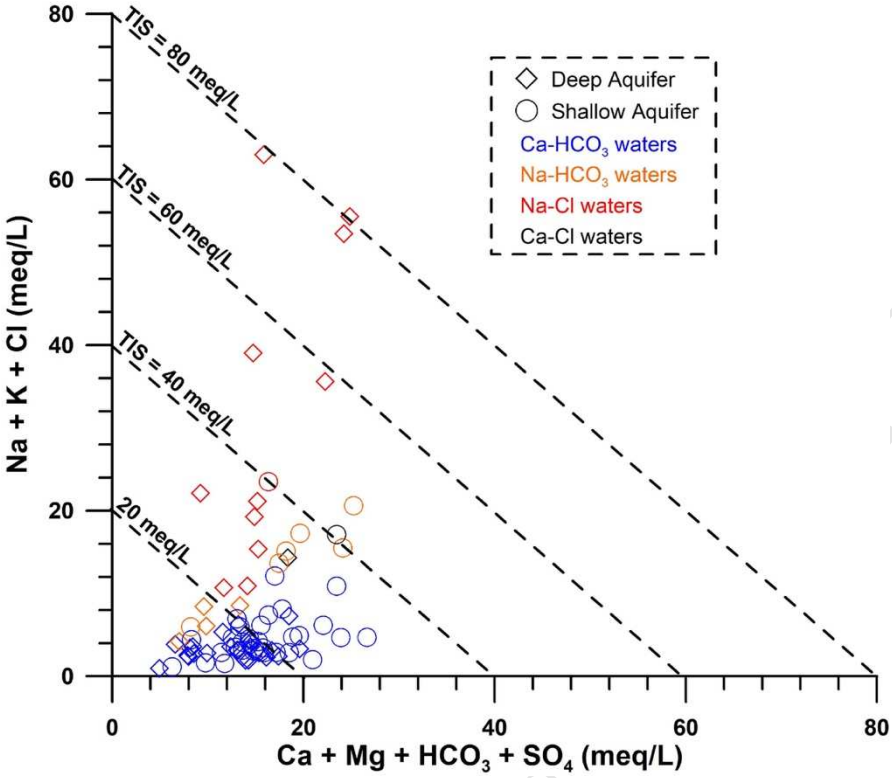

Figure 6 - Correlation diagram of Ca + Mg + HCO_3 + SO_4 vs. Na + K + Cl for the SPGS groundwaters.

In particular: (i) Ca-HCO_3 waters have the lowest TIS values and the smallest range; (ii) Na-Cl waters show the highest TIS values and the largest range; (iii) Na-HCO_3 waters have intermediate TIS values; (iv) the Ca-Cl type is represented by 2 samples only.

4.2.2 Insights gained from the physico-chemical analysis: Mixing between seawater and groundwater and ion exchange processes;

In order to explain the origin of Na-Cl, Ca-Cl and Na-HCO_3 waters we took into account the role of ion exchange processes. This processes typically occur in aquifers close to the coastline upon either seawater/brackish water intrusion or displacement of seawater by freshwater, generally of Ca-HCO_3 chemical composition (freshening) (Appelo, 1994, 1996; Appelo e Postma, 1996 and references therein; Langmuir, 1996). According to Appelo (1996) the surface sites of some solid phases (clay minerals, zeolites, etc.) in alluvial deposits act as cation exchangers. In the absence of seawater intrusion, these surface sites are saturated by Ca^{2+} (or Mg^{2+}) ions resulting from water-rock

interaction. In contrast, upon occurrence of seawater intrusion, the interaction between seawater and alluvial sediments causes the following ion exchange reactions:

$$Na^+ + Ca_{0.5}\text{-}X \rightarrow Na\text{-}X + \tfrac{1}{2}\, Ca^{2+} \quad (1)$$

$$Na^+ + Mg_{0.5}\text{-}X \rightarrow Na\text{-}X + \tfrac{1}{2}\, Mg^{2+} \quad (2)$$

where X represents a generic cation exchanger inside the alluvial sediments. As a result of reactions (1) and (2), the aqueous solution acquires Ca^{2+} and Mg^{2+} ions and lose the same amount (in equivalent units) of Na^+ and K^+ ions that saturate the cation exchanger sites. Thereby chemical composition evolves from the Na-Cl facies to the Ca-Cl facies which is represented in our data set by two samples (see above).

The reverse process occurs when Ca-HCO_3 water interact with the alluvial sediments (whose sites are saturated by Na^+ ion due to previous seawater intrusion). In this case, the reactions (1) and (2) reverse and proceed from right to left. These ion exchange processes lead to the production of the Na-HCO_3 water (10 samples, see above). For a better understanding of these ion exchange processes, they were modeled by the EQ3/6 software package (Wolery and Jarek, 2003) adopting the Vanselow convention for the cation exchanger and assuming the presence of a single exchange site. During the simulations, temperature was maintained constant at 25°C, which is a few degrees centigrade higher than average water temperature (19.8°C). Since the enthalpy of the ion exchange reactions is unknown, this is a mandatory approximation. Ion exchange upon seawater intrusion was modeled by adding progressively increasing quantities of cation exchanger, up to the maximum value of 1 mole, to 1 kg of average seawater (Nordstrom et al. 1979; Nordstrom 2000). Main results are reported in Table 4 and in Figure 7.

Table 4. Variation of the aqueous solution (average seawater) chemistry during ion exchange upon seawater intrusion. Xi represents the moles of cation exchanger added to 1 kg of average seawater.

Xi	pH	Alkalinity	Ca	Cl	C	K	Mg	Na	SO_4

		mg HCO_3/kg	mg/kg	mg/kg	mg/kg	mg/kg	mg/kg	mg/kg	mg/kg
0	7.591	113.5	392	1.87E+04	21.7	386	1.25E+03	1.04E+04	2622
5.00E-02	7.1433	103.1	1.21E+03	1.87E+04	20.7	398	1.18E+03	9.58E+03	2622
1.00E-01	6.9655	97.2	1.96E+03	1.87E+04	20.1	409	1.11E+03	8.85E+03	2622
1.50E-01	6.8609	93.3	2.64E+03	1.87E+04	19.8	420	1.04E+03	8.20E+03	2622
1.61E-01	6.8429	92.5	2.78E+03	1.87E+04	19.7	423	1.02E+03	8.07E+03	2619
2.00E-01	6.799	90.7	3.13E+03	1.87E+04	19.5	431	965	7.63E+03	2316
2.50E-01	6.7523	88.6	3.57E+03	1.87E+04	19.3	441	897	7.11E+03	2031
3.00E-01	6.7146	86.9	3.98E+03	1.87E+04	19.2	450	836	6.66E+03	1825
3.50E-01	6.6841	85.5	4.35E+03	1.87E+04	19	459	782	6.25E+03	1672
4.00E-01	6.659	84.3	4.69E+03	1.87E+04	18.9	468	735	5.90E+03	1555
4.50E-01	6.6382	83.4	5.00E+03	1.87E+04	18.9	476	693	5.58E+03	1465
5.00E-01	6.6207	82.5	5.28E+03	1.87E+04	18.8	484	657	5.29E+03	1393
5.50E-01	6.6059	81.8	5.53E+03	1.87E+04	18.7	492	625	5.03E+03	1333
6.00E-01	6.5931	81.2	5.76E+03	1.87E+04	18.7	499	596	4.80E+03	1285
6.50E-01	6.582	80.7	5.96E+03	1.87E+04	18.6	506	571	4.59E+03	1243
7.00E-01	6.5723	80.3	6.15E+03	1.88E+04	18.6	513	549	4.39E+03	1210
7.50E-01	6.5637	79.8	6.32E+03	1.88E+04	18.5	520	529	4.22E+03	1181
8.00E-01	6.5561	79.5	6.48E+03	1.88E+04	18.5	527	511	4.05E+03	1154
8.50E-01	6.5493	79.2	6.62E+03	1.88E+04	18.5	533	495	3.90E+03	1133
9.00E-01	6.5432	78.9	6.76E+03	1.88E+04	18.4	540	481	3.77E+03	1112
9.50E-01	6.5376	78.6	6.88E+03	1.88E+04	18.4	546	467	3.64E+03	1094
1	6.5326	78.4	6.99E+03	1.88E+04	18.4	552	455	3.52E+03	1079

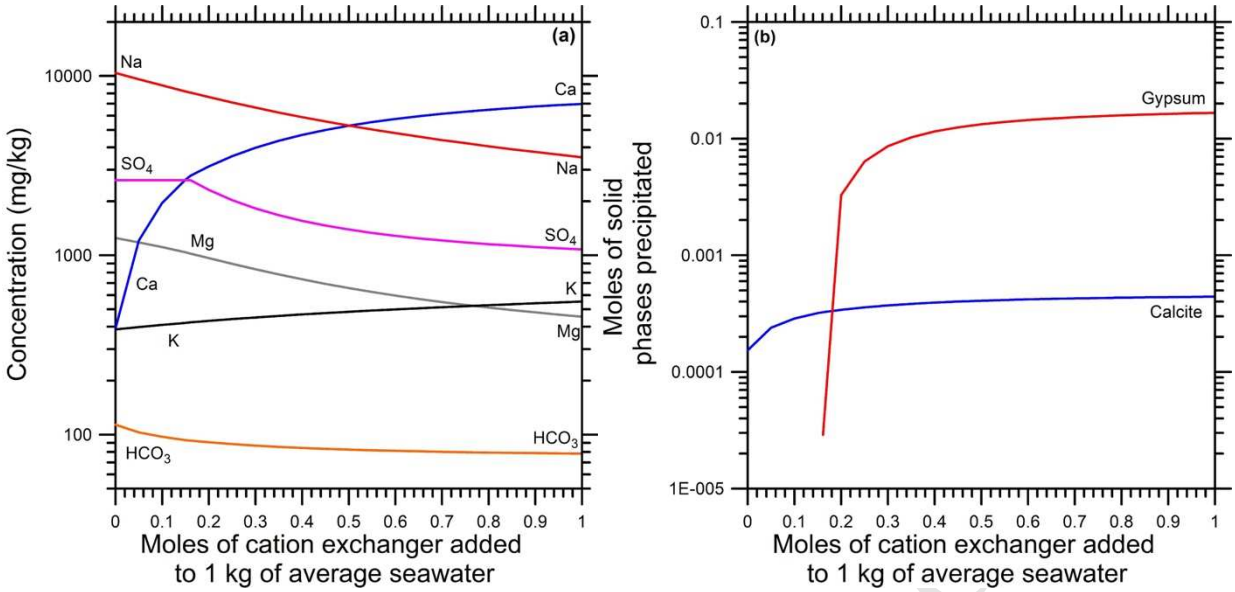

Figure 7. (a) Variation of the concentrations of major dissolved constituents and (b) Moles of solid phases precipitated as a function of the moles of cation exchanger added to 1 kg of average seawater.

At the beginning of the simulation, seawater is already strongly supersaturated with calcite (SI =0.650), which precipitates immediately, although in small quantities (Figure 7b). The interaction of seawater with increasing amounts of cation exchanger leads to increasing Ca concentration (Figure 7a), in spite of the occurrence of calcite precipitation. The separation of this mineral causes a significant decrease of bicarbonate concentration because HCO_3 << Ca. Upon addition of 0.161 moles of cation exchanger to 1 kg of aqueous solution, gypsum saturation is attained and these mineral precipitates (Figure 7b) causing a decrease of dissolved SO_4 (Figure 7a). Increase of dissolved Ca concentration is necessarily accompanied by a concurrent decrease of dissolved Na, in equivalent amounts, while aqueous Mg decreases and dissolved $K_{(aq)}$ increases.

Ion exchange upon freshwater inflow in an aquifer previously affected by seawater intrusion was modelled by adding progressively increasing amounts of cation exchanger, up to the maximum value of 0.006 moles, to 1 kg of average groundwater. Main results are reported in Table 5 and in Figure 8.

Table 5. Variation of the aqueous solution (average groundwater) chemistry during ion exchange upon groundwater inflow into an aquifer previously affected by seawater intrusion. Xi represents the moles of cation exchanger added to 1 kg of average groundwater.

Xi	pH	Alkalinity	Ca	Cl	C	K	Mg	Na	SO_4
		mg HCO_3/kg	mg/kg	mg/kg	mg/kg	mg/kg	mg/kg	mg/kg	mg/kg
0	7.4978	157.4	60.8	17.5	32.7	1.69	17.8	15.9	103.7
5.00E-04	7.5329	158.8	55.4	17.5	32.9	1.69	15.4	27.2	103.7
1.00E-03	7.5729	160.3	49.9	17.5	33	1.68	13.1	38.2	103.7
1.50E-03	7.6188	161.9	44.4	17.5	33.2	1.68	11.1	49	103.7
2.00E-03	7.6715	163.6	38.8	17.5	33.3	1.68	9.23	59.5	103.7
2.50E-03	7.7324	165.4	33.4	17.5	33.5	1.67	7.56	69.7	103.7
3.00E-03	7.8033	167.3	28	17.5	33.7	1.67	6.07	79.4	103.7
3.50E-03	7.8857	169.3	22.9	17.5	33.9	1.66	4.76	88.4	103.7
4.00E-03	7.981	171.3	18.3	17.5	34.1	1.65	3.64	96.7	103.7
4.50E-03	8.0893	173.5	14.2	17.5	34.3	1.64	2.72	104	103.7
4.71E-03	8.1369	174.4	12.7	17.5	34.4	1.64	2.4	107	103.7
5.00E-03	8.1453	174.4	10.5	17.5	34.4	1.63	1.97	110	103.7
5.50E-03	8.1571	174.4	7.61	17.5	34.4	1.61	1.41	114	103.7
6.00E-03	8.1659	174.4	5.55	17.5	34.4	1.59	1.01	117	103.7

First, it should be noted that the amounts of added cation exchanger, which are needed to cause significant effects on groundwater composition, are much smaller than those needed to determines important consequences on seawater chemistry (see seawater intrusion simulation above). These differences are evidently due to the different salinity, in equivalent units, of the two aqueous solutions. Also, in this second model, calcite precipitates immediately (Figure 8b), even if in small quantities, decreasing progressively during the simulation until calcite precipitation ends upon addition of 0.0045 moles of cation exchanger to 1 kg of aqueous solution. Calcite precipitation has a modest effect on aqueous solution composition, which is dominated by Na/Ca exchange, with a progressive decrease in Ca concentration and a corresponding gradual increase in Na concentration in equivalent units (Figure 8a). Aqueous Mg undergoes a considerable decrease during the simulation, while dissolved K experiences a moderate decrease.

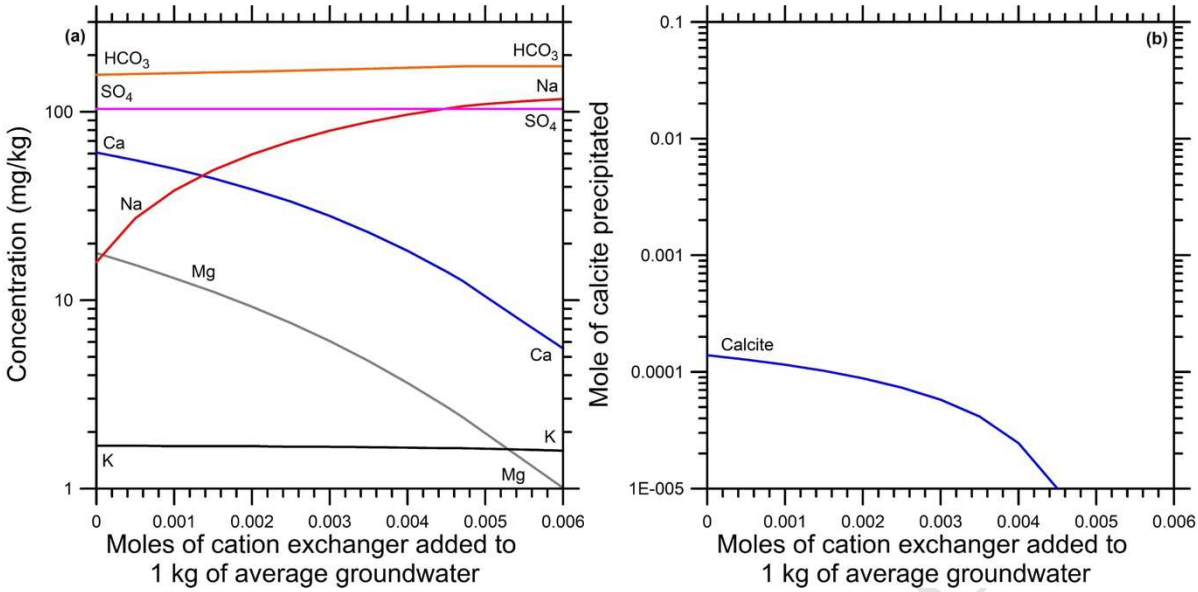

Figure 8. (a) Variation of the concentrations of major dissolved constituents and (b) Mole of calcite precipitated as a function of the moles of cation exchanger added to 1 kg of average groundwater.

The results of the two simulations are reported in the two correlation diagrams of Na+K vs. Ca+Mg (Figure 9) showing that ion exchange processes, during both seawater intrusion and freshening take place at constant TIS values, apart from a modest decrease in salinity in the first process, due to gypsum precipitation. In fact, both reaction paths are parallel to the iso-salinity lines in the two diagrams but have opposite direction.

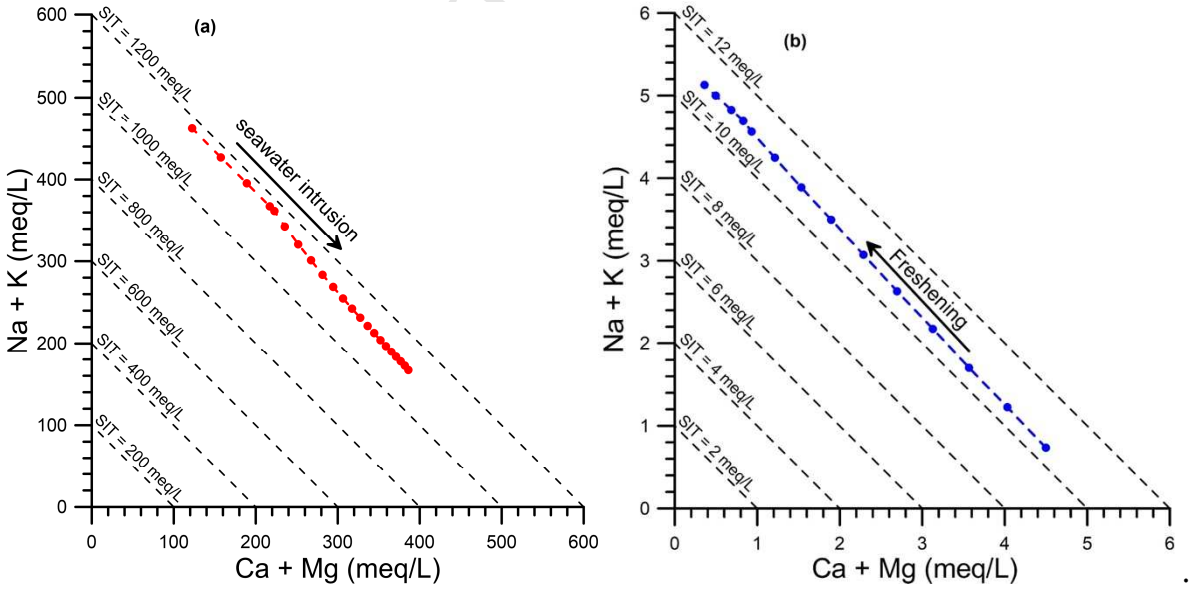

Figure 9. Correlation diagrams of Na+K vs. Ca+Mg showing the results of geochemical modeling for ion exchange processes triggered by seawater intrusion and freshening.

The triangular diagram of Cl-HCO_3-SO_4 (Figure 10a) shows that ion exchange effects of seawater intrusion and freshening are nil to negligible on the relative contents of major anions. The small observed changes are probably due to the precipitation of solid phases, such as calcite and gypsum, rather than to ion exchange processes.

In contrast, the triangular diagram of (Na+K)-Mg-Ca (Figure 9b) highlights the significant effects of ion exchange accompanying seawater intrusion and freshening on the relative contents of major cations, mainly on the Na/Ca ratio. Note the opposite direction of the two reaction paths.

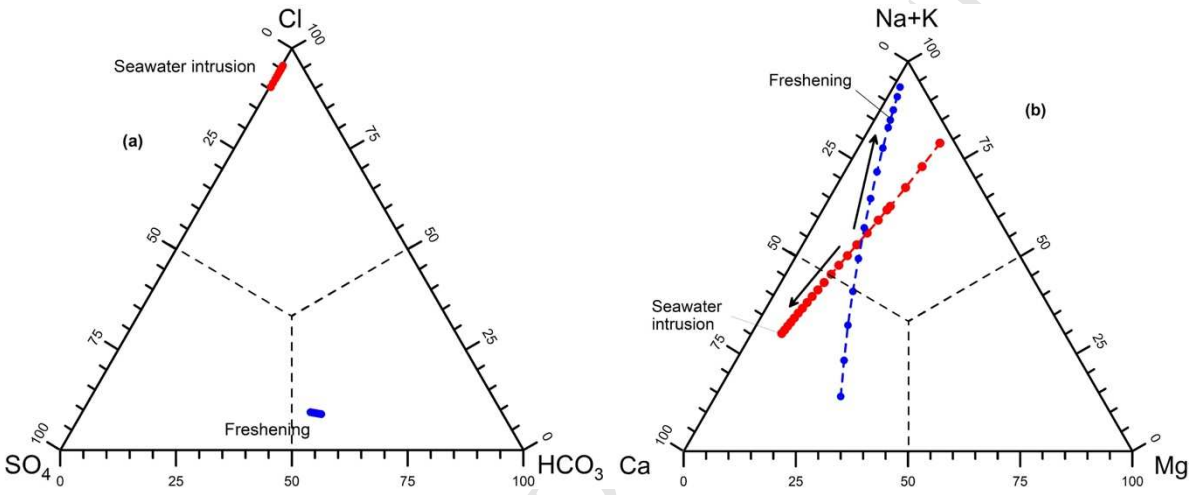

Figure 10. Triangular plots of (a) major cations and (b) major anions, both prepared starting from concentrations in equivalent units, showing the effects of ion exchange processes accompanying seawater intrusion and freshening.

In the Ca vs. Cl and Na vs. Cl diagrams (Figure 11) chloride, which is the main mobile (or conservative or inert) constituent in natural waters (since once added to the aqueous solution it remains there), is plotted against Na^+ and Ca^{2+}, which are the two cations most affected by ion exchange processes. In all diagrams, two mixing lines between average seawater and groundwater endmember belong to the Ca-HCO_3 facies are drawn for each aquifer. Samples (P56-P47 belonging to the HU1 aquifer and P12- P15 to the HU3 aquifer) highlight relatively low chloride concentrations and low and high calcium contents, respectively.

Mixing lines were constructed using the following mass balance equation, varying the seawater fraction x_{SW}:

$$C_{i,MW} = C_{i,SW} \cdot x_{SW} + C_{i,GW} \cdot (1 - x_{SW}) \quad (3)$$

where $C_{i,MW}$, $C_{i,SW}$, and $C_{i,GW}$ are the concentrations (in meq/L) of i-th component in the mixture, in average seawater, and in the groundwater endmember, respectively.

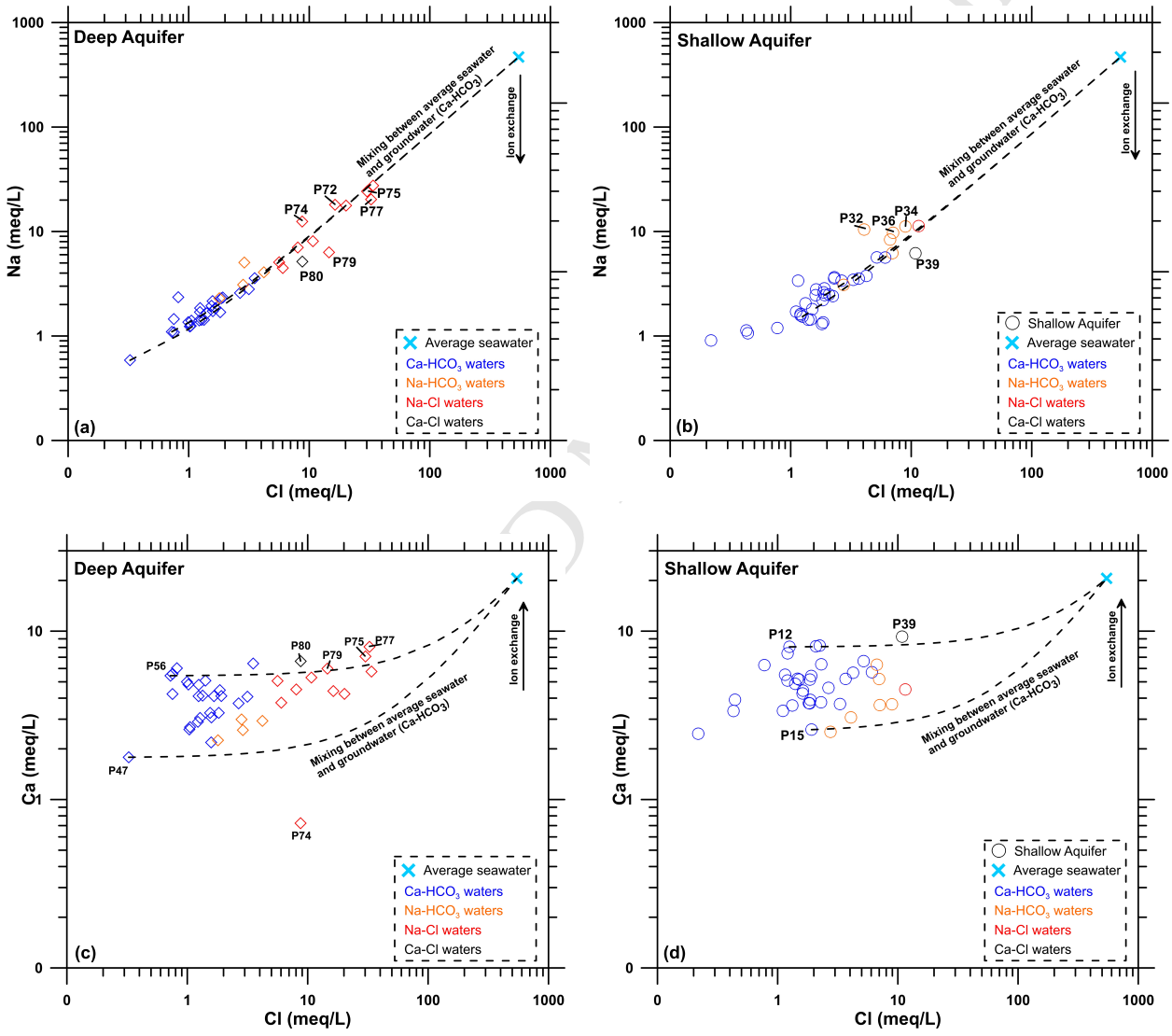

Figure 11 - Log-log diagrams of Na vs. Cl and Ca vs. Cl for the SPGS aquifers (HU1 and HU3) also showing average seawater and the mixing lines between average seawater and the groundwater endmember (samples P56 and P47 - HU1 aquifer; P12 and P15 – HU3 aquifer). The arrow "ion exchange" refers to the effects expected for seawater intrusion.

In the Na vs. Cl diagrams (Figures 11a and 11b), the seawater dilution lines are very close to each other because sodium concentration of samples (P47-P56 and P15- P12) are comparable (0.59-1.10

meq/L and 2.46-1.53 meq/L respectively). In the deep aquifer, ion exchange effects due to seawater intrusion (loss of sodium with respect to the mixing lines) are not very clear even if the sample belonging to the Ca-Cl type (P80) and some samples of the Na-Cl type fall below the mixing lines (P75, P77 and P79). In contrast, Na-HCO_3 samples fall either along the mixing lines or above them as expected for ion exchange due to freshening. On the other hand, in the shallow aquifer (Figure 11b), ion exchange effects due to seawater intrusion are almost completely absent except for sample belonging to the Ca-Cl type (P39). Much more evident are the freshening effects in the Na-HCO_3 samples falling above the mixing lines.

In the correlation plots Ca vs. Cl (Figures 11c and 11d), the seawater - groundwater mixing lines are clearly separated due to the wide range of Ca concentration (1.78 - 5.44 meq/L and 2.60 - 8.07meq/L for samples P47, P56, P15 and P12 respectively). For the deep aquifer, ion exchange due to seawater intrusion is evident in sample belonging to the Ca-Cl chemical type (P80) and to those of Na-Cl falling above the mixing lines (P75, P77 and P79). The opposite ion exchange effects, due to freshening, are shown by some Na-HCO_3 samples falling close to the lower mixing line. The anomalous low Ca content of sample P74 may be explained by calcite precipitation.

Shallow aquifer (Figure 11d) highlights not very clear effects due to seawater intrusion. Only sample P39, belonging to the Ca-Cl type, falls above the mixing line. As said before, much more evident are the freshening effects in the Na-HCO_3 samples falling close to the lower mixing line.

Freshening seems concentrated in narrow zones in which higher rainfall infiltration or fresh surface water leakage from drainage network occurs, as verified merging DSMs, DTM and on site information.

In the Mg vs. Cl diagrams (Figures 12a and 12b), most samples fall along the seawater - groundwater mixing lines and there are no evidences of ion exchange processes.

The correlation diagrams of K vs. Cl (Figures 12c and 12d) suggest that the potassium distribution in the SPGS HU1 aquifer is likely controlled by mixing between groundwater and marine waters. In

fact, high K concentration are recognized predominantly in samples belonging to the Na-Cl chemical type whereas, Ca-HCO_3 samples fall in proximity of the mixing lines.

On the other hand, potassium distribution in the SPGS HU3 aquifer is probable controlled by both mixing between groundwater and marine waters and use of fertilizers in agriculture (Datta et al., 1997; Jalali, 2007; Shamrukh et al., 2001; Skowron et al., 2018; Vespasiano et al., 2016a), which determines moderate excesses of K in Ca-HCO_3 samples compared to the seawater dilution line.

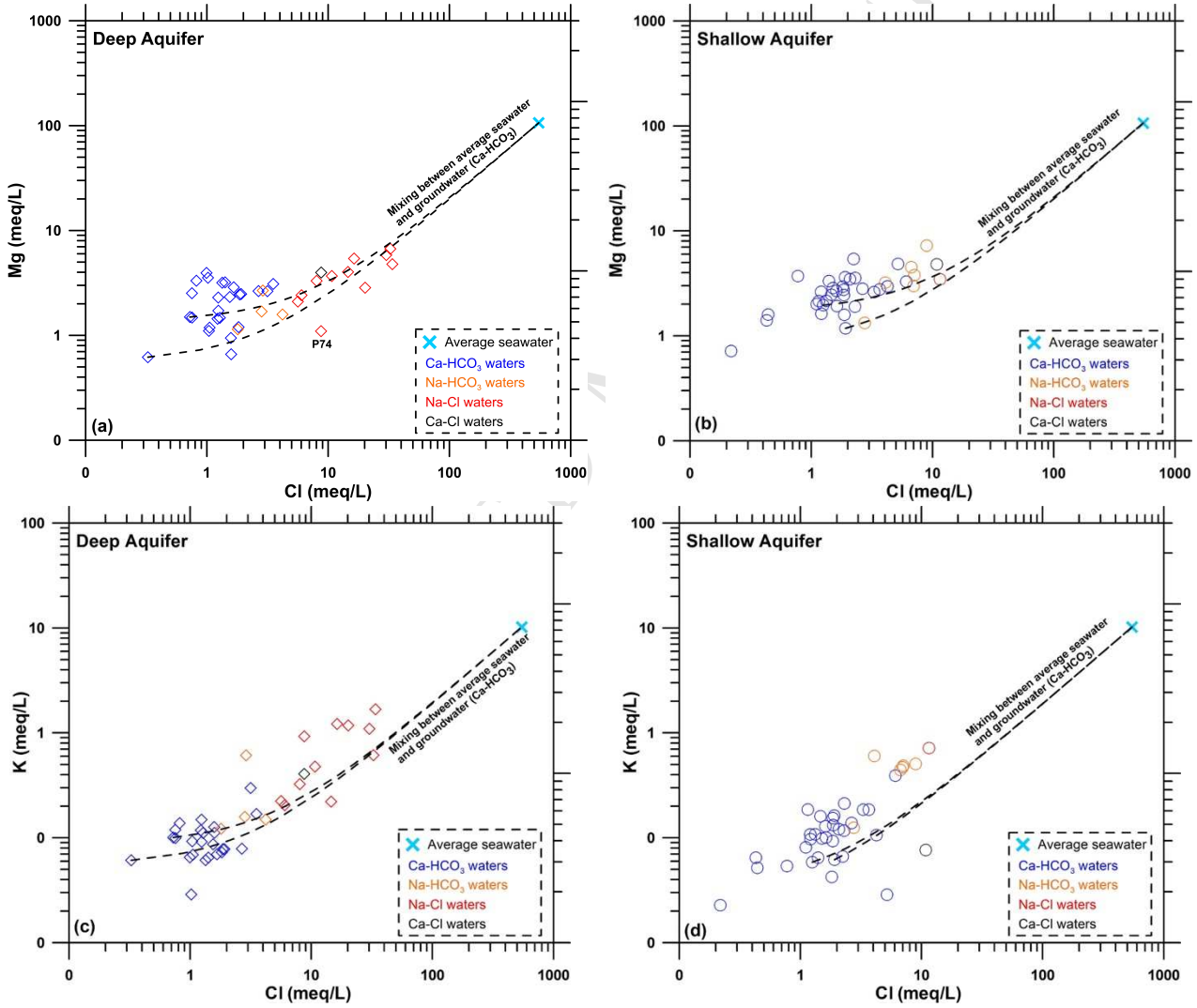

Figure 12. Log-log diagrams of Mg vs. Cl and K vs. Cl for the SPGS aquifers, also showing the mixing lines between average seawater and groundwater.

Although the Cl concentrations are very low in both the HU3 and HU1 aquifer we can conclude that only the deep aquifer is moderately affected by ion exchange processes. This could be related to the

relatively low fraction of seawater involved in the mixing phenomena. The seawater fraction, x_{SW}, in each sample was computed by solving the chloride mass balance equation with respect to x_{SW}:

$$x_{SW} = \frac{Cl_{MW} - Cl_{GW}}{Cl_{SW} - Cl_{GW}} \quad (4)$$

where MW, GW and SW refer to the seawater contaminated groundwater, the pure groundwater and seawater, respectively. The Cl content of the pure groundwater was sets equal to the lowest Cl content, 11.57 mg/kg (sample P47). The chloride content of seawater was considered equal to the average value of the Ionian Sea, 21339 ± 134 mg/kg (1σ), which was calculated based on the available data (Pierre, 1999; Schmidt et al. 1999; Stenni et al. 1995). The computed x_{SW} values for the HU1 aquifer generally vary between 0.01 and 0.02 with peaks of 0.027 in P72, 0.034 in P69, 0.052 in P75, 0.057 in P77 and 0.059 in well P70. To be noted that (i) wells P69, P70, and P72 are positioned in a small area close to the mouth of the Crati River at <1 km from the river itself and 1.4-2.0 km from the coastline; (ii) well P75 is situated close to the mouth of the Trionto River at <2 km from the river itself and 1.3 km from the coastline. Only well P77 is positioned at <1 km from the Crati river and 5.0 km far from the coastline. Based on the location of these wells, seawater intrusion is the most probable explanation for their high chloride concentration and related geochemical characteristics, whereas halite dissolution appears to be an unlikely chloride source except for sample P77 due to its location relatively far from the coastline.

4.2.3 Stable isotope discussion

Starting from the analytical $\delta^{18}O$ and $\delta^{2}H$ values of each seawater-contaminated groundwater, the corresponding isotope values (indistinctly indicated by the symbol δ_{GW}) of each pure groundwater (i.e., before mixing with seawater) were computed by solving the isotope balance equation for δ_{GW}:

$$\delta_{GW} = \frac{\delta_{MW} - \delta_{SW} \cdot x_{SW}}{1 - x_{SW}} \quad (5)$$

in which δ_{MW} and δ_{SW} are the isotope values of the seawater-contaminated groundwater and local seawater, respectively, and x_{SW} is the seawater fraction obtained through equation (4). The average isotope values of local seawater were constrained using the data available for the Ionian Sea (Gat et al. 1996; Pierre, 1999; Schmidt et al. 1999; Stenni et al. 1995) at $\delta^{18}O = +1.43 \pm 0.10‰$ and $\delta^{2}H = +8.05 \pm 0.38‰$.

The computed isotope values of pure groundwaters define the local meteoric line:

$$\delta^{2}H = 6.02 \cdot \delta^{18}O + 0.16, \quad (6)$$

which diverges substantially from the Southern Italy meteoric line (Longinelli and Selmo, 2003)

$$\delta^{2}H = 6.97 \cdot \delta^{18}O + 7.317, \quad (7)$$

as shown by Figure 13.

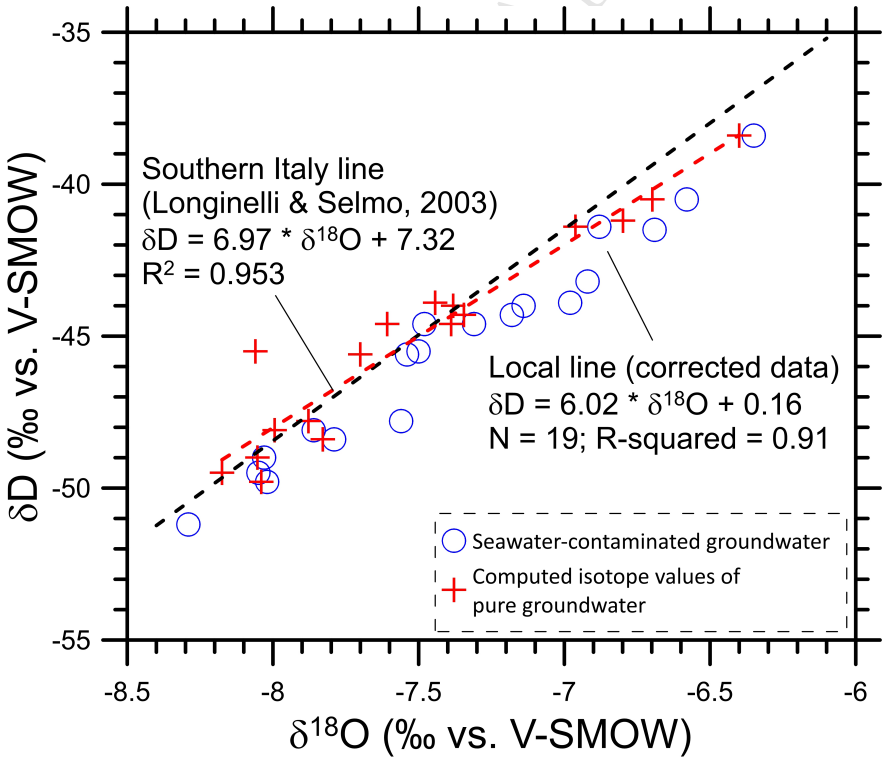

Figure 13 - Binary diagrams $\delta^{18}O$ vs. δD.

The average infiltration altitude (Hi, m asl) of SPGS aquifers was calculated by means of the following equations:

$$H_{i,^{18}O} = -\frac{\delta^{18}O + 5.25}{0.00210} \quad (8)$$

$$H_{i,^{2}H} = -\frac{\delta^{2}H + 26}{0.0145} \quad (9)$$

which were obtained using the Small Spring Method, SSM (Vespasiano et al. 2015c).

In general, average infiltration altitudes given by $\delta^{2}H$ values (equation 13) are higher than those given by $\delta^{18}O$ values. Adopting the $\delta^{18}O$ values resulted average infiltration altitudes of 1210±136 m asl and 757±166 m asl for HU1 and HU3 aquifers respectively.

The average infiltration altitudes of 757±166 m asl for the shallow (HU3) aquifer are likely affected both by local rains and exchanges with the fluvial bodies that mediate the isotopic compositions of the waters coming from the entire basin of the Crati river..On the other hand, the influence of local precipitations appears to be less important for the recharge of the deep aquifer, which seems to be supplied essentially from the Pollino and Sila massifs.

Table 6. Analytical ‰^{18}O and ‰^{2}H values of seawater-contaminated SPGS groundwaters, computed $\delta^{18}O^*$ and $\delta^{2}H^*$ values of corresponding pure groundwaters, and average infiltration altitudes, Hi, calculated from the $\delta^{18}O^*$ and $\delta^{2}H^*$ values. In bold samples representative of the deep aquifer.

N.	Cl	Chemical type	‰^{18}O	‰^{2}H	‰$^{18}O^*$	‰$^{2}H^*$	Hi,$^{18}O^*$	Hi,$^{2}H^*$
	mg/kg		‰ vs. V-SMOW		‰ vs. V-SMOW		m asl	
P42	56	Ca-HCO_3	-8.02	-49.8	-8.04	-49.92	1328	1650
P65	64	Na-HCO_3	-8.03	-49	-8.05	-49.14	1335	1596
P66	100	Na-HCO_3	-7.79	-48.4	-7.83	-48.64	1228	1561
P76	199	Na-Cl	-7.31	-44.6	-7.39	-45.07	1018	1315
P73	285	Na-Cl	-8.05	-49.5	-8.17	-50.26	1393	1673
P74	310	Na-Cl	-7.48	-44.6	-7.61	-45.36	1123	1335
P80	310	Ca-Cl	-7.86	-48.1	-7.99	-48.91	1307	1580
P71	380	Na-Cl	-7.54	-45.6	-7.70	-46.56	1167	1418
P72	580	Na-Cl	-7.14	-44	-7.38	-45.46	1015	1342
P69	716	Na-Cl	-7.56	-47.8	-7.88	-49.77	1251	1640
P75	1070	Na-Cl	-6.98	-43.9	-7.44	-46.76	1044	1432
P70	1200	Na-Cl	-7.5	-45.5	-8.06	-48.86	1338	1576
P42	56	Ca-HCO_3	-8.02	-49.8	-8.04	-49.92	1328	1650
P65	64	Na-HCO_3	-8.03	-49	-8.05	-49.14	1335	1596
P66	100	Na-HCO_3	-7.79	-48.4	-7.83	-48.64	1228	1561

P32	144	Na-HCO_3	-6.35	-38.4	-6.40	-38.70	548	876
P8	216	Ca-HCO_3	-6.88	-41.4	-6.96	-41.89	815	1096
P35	237	Na-HCO_3	-6.71	-41.2	-6.80	-41.74	737	1085
P34	317	Na-HCO_3	-6.58	-40.5	-6.70	-41.21	689	1049
P38	409	Na-Cl	-7.18	-44.3	-7.34	-45.30	998	1331

4.3 Coastal aquifer hydrogeological modelling

The use of groundwater resources in Calabria began in the 70s and gradually increased through the drilling of several wells, now in the order of tens of thousands. Today almost all fresh water used in Calabria comes from groundwater (Polemio et al. 2013). This resource is subject to a quantitative degradation due to both the increase of water demand and climate change; groundwater overexploitation of regional aquifers adds risks of groundwater quality degradation due to seawater intrusion, especially in the case of SPGS (Polemio et al. 2004, Polemio and Casarano 2004).

To investigate these phenomena with management purposes, a 3D hydrogeological conceptualisation to support the numerical modelling of the SPGS aquifers was realised. The conceptualised area is bordered to the north and north-east by the Mesozoic limestone rocks of Pollino Massif and to the south and southwest by the foothills of the Paleozoic crystalline lithotypes of the Sila Massif and the Ionian Coastline.

The hydrogeological conceptualisation consists of the three hydrogeological units, distinguished in the previous chapter, from the top to the bottom (Figure 14): 1) HU3, sand and clay complex, formed by alluvial deposits, characterized by permeability from medium to high, hosting the SSPGS aquifer; 2) HU2, clay and silt complex, not outcropping in the study area, to be considered at very low permeability; 3) HU1, sand and conglomerate complex, which includes a not negligible cohesive fraction, characterized by medium permeability.

Apart from natural recharge due to direct rainfall infiltration, the SPGS aquifers receive water inflow from boundaries. Considering boundary conditions, focusing mainly on permeability limits and main close aquifers, relevant inflow should be considered due to leakage from adjacent aquifers

of the Sila and Pollino massifs. The role of the natural drainage network, ranging from Crati River to a number of secondary ephemeral watercourses (called *fiumare*), is due to the prevailing coarse grain size of alluvial beds (HU3b), which is able to permit water exchange with SSPGS aquifer. Using DTM data, specific data collection, surveys, and data analysis were realised to assess geometrical features, including thickness and grain size, of riverbeds and river water head. Due to the geometrical peculiarities of drainage network and the high variability of river stages in SPGS, this exchange should be considered spatially and timely variable but, in any case, not able to affect significantly the hydrological balance of SPGS aquifers.

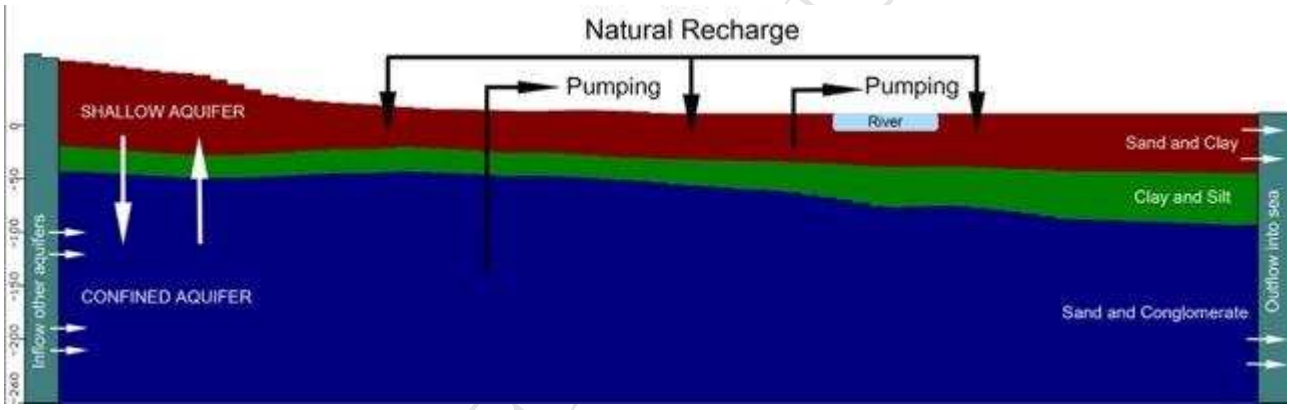

Figure 14 – Conceptual model and hydrogeological complex

On theses bases, the model was calibrated and validated with data from thirties to 2000 using historical data, mainly climate and piezometric data. The model area extension is about 365 km^2.

The Equivalent Porous Medium approach (EPM) was chosen for the numerical model, as it is particularly efficient to represent the flow and transport on a regional scale and for resource management purposes, where high-resolution results are less important than an overall assessment of the state of groundwater resources (Langevin 2003; Pisinaras et al. 2007; Zuffianò et al. 2016). Using EPM, the discretization should be coarse enough to be appropriate for the basic hypothesis of equivalent continuous porous medium. The modelled area was uniformly discretized into a finite

difference grid of 97,735 cells of 240 m x 350 m. The model was divided into five layers of variable thicknesses, based on previously described geological knowledge (Figure 15).

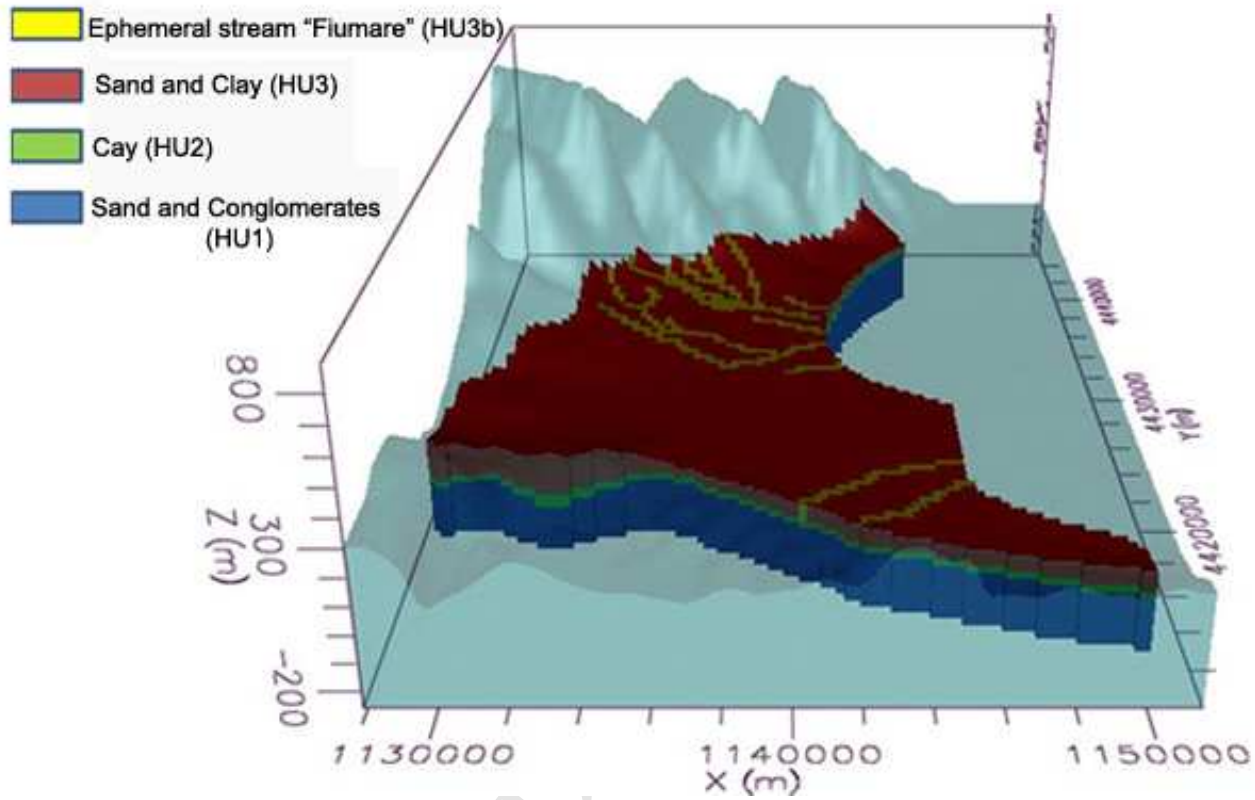

Figure 15 – 3d view of DTM and of the SPGS hydrogeological conceptualisation, using hydrogeological complexes, and grid discretisation ("fiumare" describes geometry and location of riverbeds).

The computer codes MODFLOW and SEAWAT were selected for numerical groundwater modelling (Guo and Langevin 2002; McDonald & Harbaugh AW 1988).

As boundary condition a Dirichlet condition (Constant Head Boundary) for the coastline and for the west border of Pollino and Sila Massifs were used, while for the Crati and Coscile rivers the Cauchy condition was used.

The necessary hydrogeological parameters, hydraulic conductivity and storage coefficients, were defined discussing field surveys, tests and laboratory data together with an extensive literature research (as main considered references Anderson & Woessner, 1992; Davis, 1969; Domenico, 1972; Johnson, 1967; Jumikis, 1962; Martin & Frind, 1998; Rehm, 1980). Grain size laboratory

tests and 42 Lefranc tests were main measured data used for the preliminary assessment of hydrogeological parameters.

Climate data were used for the assessment of the natural recharge: monthly data of rainfall and temperature over the period 1930-1975, for a total duration of 45 years, were selected as a period free from relevant effects of climate change (Polemio and Casarano 2004). The spatial assessment of necessary climate variables was realised in an area larger than the study area, to maximize the reliability of recharge assessment: 11 rainfall gauges, 3 of which include a thermometric probe, were selected for this purpose. The linear correlation functions between mean annual rainfall (P, mm) and temperature (T, °C) from a side and altitude (z, m asl) from the other side were defined applying the least squares method:

$$P = 562.08 + 3.9z \quad (10)$$

$$T = 17.39-0.0034z \quad (11)$$

The P and T calculation was applied for each model cell using mean cell z value, obtained by DTM. The mean annual rainfall increases from NW to SE, with a spatial mean value of 700 mm, while the mean annual temperature varies between 14.2 and 17.3 °C.

The mean annual actual evapotranspiration (E, mm) was calculated in each cell using the Turc method, modified to be reliable for Italian aquifers (Cotecchia et al. 1990). On this basis, the mean annual effective infiltration (I, mm) was calculated in each cell multiplying the effective rainfall, equal to P-E, by the infiltration coefficient for each hydrogeological complex, on the basis of literature data (Celico, 1988; Civita, 2005). The infiltration does not exceed 100 mm; the spatial mean value is 29 mm for a total annual volume of infiltration equal to 2×10^8 m^3. The calculation of the direct recharge shows its contribution to the hydrological balance of coastal plain aquifers is expected to be relatively low. Other sources of water input, as the leakage from other neighbouring

aquifers, appear should be relevant, as proposed by previous authors (Guerricchio et al., 1976; Polemio and Luise, 2007; Tazioli, 1986;).

4.3.1 Steady-state model and Calibration

The first simulation was performed to define the steady-state groundwater flow and 3D salinity field to simulate nearly natural steady-state conditions (no climate change, negligible anthropogenic effects). In this simulation, the piezometric surface of thirties was used to define the initial head values (Polemio et al. 2004b), steady-state recharge was assumed, and no discharging wells were considered. The hydraulic conductivity K was calibrated using a numerical code (PEST) integrated in MODFLOW. Eighteen piezometric wells, with data from the 1930s, were used for calibration (Table 7). The statistics of K (m/s) calibration analysis are (Zheng and Bennett 2002): mean residual error -0.12, mean absolute residual error 0.45, normalised root mean squared of residual errors 11.89%, correlation coefficient 0.903 (linear regression between observed and calculated values), and standard deviation 0.3.

The results confirmed the relevance of the inflow due to Sila and Pollino leakage and showed a water exchange between the shallow aquifer and the deep aquifer far from the coast, in the inland portion of the plain, where the aquiclude thickness is lower.

Hydrogeological complex	**Hydraulic conductivity (m/s)**		
		Initial value	Calibrated value
Sand and clay (HU3)	kx	10^{-4}	$3\ 10^{-3}$
	ky	10^{-4}	$3\ 10^{-3}$
	kz	10^{-5}	$3\ 10^{-4}$
Clay and Silt (HU2)	kx	10^{-8}	10^{-9}
	ky	10^{-8}	10^{-9}
	kz	10^{-9}	10^{-9}
Sand and conglomerate (HU1)	kx	$5\ 10^{-5}$	$3.25\ 10^{-5}$
	ky	$5\ 10^{-5}$	$3.25\ 10^{-5}$
	kz	$5\ 10^{-6}$	$1.1\ 10^{-6}$

Table 7 – Calibration of the hydraulic conductivity for each hydrogeological unit.

In addition, using MODPATH code (https://water.usgs.gov/ogw/modpath/), a particle-tracking code based on MODFLOW, the velocity of groundwater was also calculated. Focusing on the deep aquifer, the maximum value of Darcy velocity was about 1.1 x 10^{-6} m/s (roughly 0.1 m/day), while the residence time in the deep aquifer was rated between 250 and 500 years.

The output of the steady-state flow model was used as input for the density-dependent model using the SEAWAT code. A constant-concentration boundary condition was used for coastal cells. The constant concentration (salinity) was assumed equal to 39,500 mg/L along the Ionian Coast (Grauel and Bernasconi, 2010). Mean groundwater salinity was assessed for each aquifer and used as initial cell values; on this basis, a steady state or initial 3D spatial distribution of groundwater salinity of was calculated, to be used as reference in the next scenarios (Figure 16a). This distribution is coherent with historical data (Figure 1, Casmez 1967)

4.3.2 Seawater intrusion and transient model from 1979 to 2020

Anthropogenic changes and the withdrawals for irrigation purposes were considered for next transient simulations. 1781 pumping wells were activated, subdivided in irrigation, industrial and civil used (Casmez, 1967, ISPRA public geodatabase of borehole data on http://portalesgi.isprambiente.it/it/categorie-db/sondaggi). A well discharging 80 L/s was also implemented where the national archaeological site of ancient Sybaris town is located. In fact, the dig, deep up to the level Roman town is under the current sea level, so a continuous underground drainage system is used by decades to maintain the piezometric surface below the excavation level.

Starting from 1979, an annual step elaboration was performed. For every step, discharges and climate data were modified. From 1989, 132 new pumping wells (ISPRA geodatabase) were added to the model. The wells are uniformly distributed throughout the area with variable flow rates between 0.25 and 30 L/s. The specific depth and the screens position were defined for each well. Climate change effects on the region were also considered (Polemio and Casarano 2004).

Some gaps of data availability were suffered from 2001, mainly concerning groundwater discharge and secondly climate data. A slight predictive scenario was defined from 2001 to 2020, as yearly transient step. In this scenario, predicted changes in rainfall, temperature, sea level, and seawater salinity were included, based on a wide literature research. A temperature variation of +0.9 °C, as mean annual spatial value of the study area, and a rainfall variation of -3.9%, referred to mean spatial value, were implemented in the whole scenario (Alpert et al. 2008; Gibelin and Déqué 2003; Giorgi and Lionello 2008; Goubanova and Li 2007; Polemio and Casarano 2004; Ragab and Prudhomme 2002). On this basis, the recharge was recalculated with a yearly linear variation. The variation of evapotranspiration was assessed as percentage of mean value (1930-1975) to be applied to increase the well discharge with a linear year approach. An increase in seawater salinity approximately equal to 0.005 g/L per year is also expected; it was implemented for the period 2010-2020 (Adani et al. 2011; Tsimplis et al. 2008).

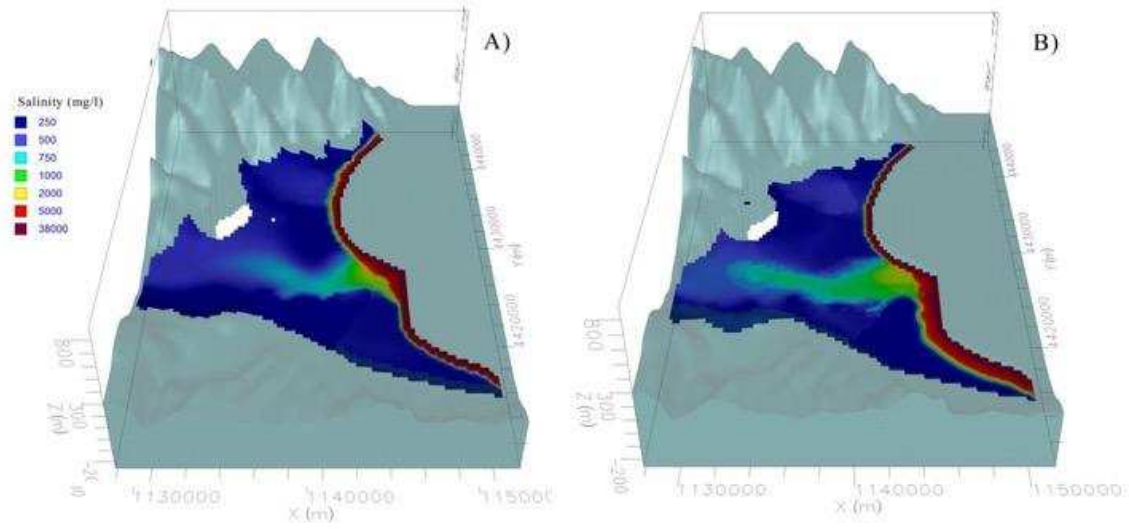

Figure 16 - 3d view of shallow groundwater salinity: A) steady state; B) expected in 2020.

The calculated salinity map of the shallow aquifer shows an average inland or lateral intrusion effect on a strip large up to of 1.4 km, with respect to the steady-state simulation (Figure 16b). In

addition, with reference to the Sybaris archaeological dig and pumping, the model shows high localized effects of seawater intrusion, due to upconing.

The numerical simulations, as a whole period of 91 years (1930 - 2020), show a qualitative and quantitative degradation. In terms of quality/salinity degradation, the effects lateral seawater intrusion seems relevant in the SSPGS aquifer, especially in the central- southern coastal sector and along the main riverbed (Crati River), where negative effects are observed far from the coast. A relevant up-coning was highlighted in the Sybaris archaeological area, involving the DSPGS aquifer (**Figure 17**).

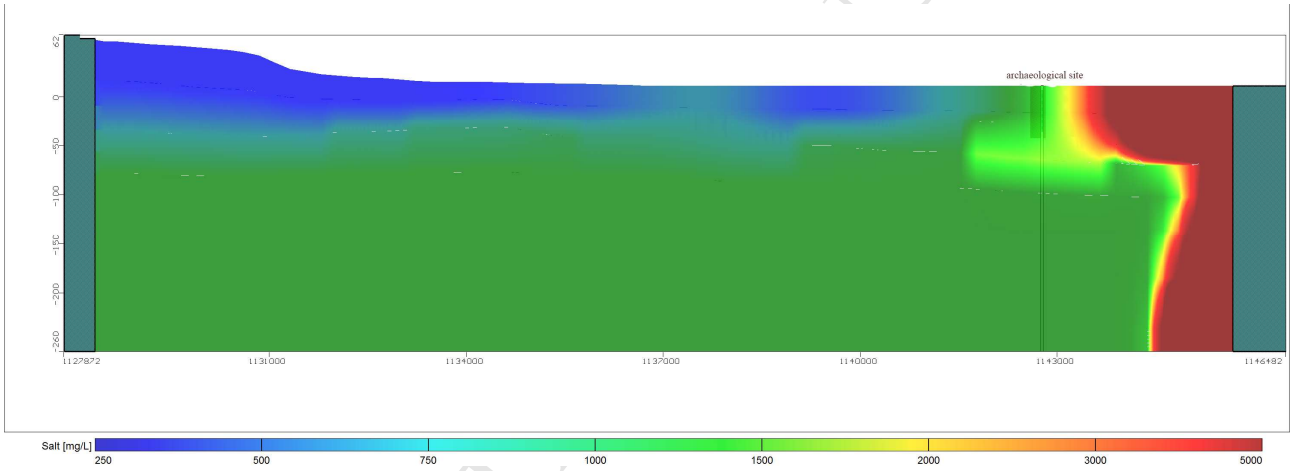

Figure 17 - W-E section: lateral intrusion and up-coning effect under the Sybaris archaeological site (Ionian Sea on the right or Eastern side of the figure)

5. Conclusions

The SPGS consists of a complex association of fluvial, alluvial fan and deltaic depositional systems. In detail, in the middle plain sector, the Crati Delta represents the main hydrostratigraphic unit. The delta evolution is strictly related to the Holocene post-glacial sea level rise overlapping to local factors as subsidence and tectonic (Cianflone et al. 2018). The hydrostratigraphic framework in the deltaic area consists of a surface layer characterized by the heteropical transition between fluvial, deltaic and shore-zone sediments (HU3 - shallow aquifer) overlay wedge-shaped fine-grained deposits (HU2 - aquitard), related to the post-glacial transgression, which lie on top of a late

Pleistocene coarse-grained coastal plain (HU1 - deep aquifer). We suppose that the confined aquifer is limited to the area of the plain Holocene evolution and its landward boundary coincides with the maximum inland extension of the early Holocene fine-grained deposits.

The upstream sectors of Crati and Coscile Rivers represent two alluvial valleys filled by fluvial deposits. The Crati and Coscile are two mixed-load meandering fluvial systems, which create a "jigsaw puzzle" style of facies and hydrostratigraphic complexity (Galloway and Sharp, 1998a, 1998b and references therein). The northeastern sector of the study area is instead characterized by big alluvial fans related to ephemeral streams with a prevalent coarse-grained bed load (Saraceno, Satanasso and Raganello Streams). These hydrostratigraphic units can be correlated to the "jigsaw-puzzle" systems (Galloway and Sharp, 1998a, 1998b). In the areas between the alluvial fans, the main deposits consist of overbank or lagoon fine-grained sediments with isolated coarse-grained deposits due to processes of crevasse. In these sectors, a "labyrinth" style of facies (Galloway and Sharp, 1998a, 1998b) is present. In the southern sector, also characterized by the presence of alluvial fans, the hydrostratigraphic pattern is very similar to the northeastern one.

The hydrostratigraphic framework is strictly related to the middle Pleistocene-Holocene evolution of the SPGS. In detail, the uplift occurred along plain boundaries, as testified by various orders of marine terraces, and triggered the alluvial fans development. Since the late Pleistocene, the post-glacial transgression and the Crati Delta progradation controlled the SPGS hydrostratigraphic architecture.

Based on the above discussion it is possible to propose the following hypothesis about the origin of the chemical types present in the studied area, briefly summarizing their salient features.

The Ca-HCO_3 chemical type is characterized by a TIS comprised between 6 and 34 meq/L and is the most represented, comprising 56 samples. These waters are probably generated by calcite dissolution, a mineral phase that dissolves very quickly (e.g., Apollaro et al. 2012; Vespasiano et al. 2016b, 2016c; Marini, 2006 and references therein) and is very frequent in the study area, as a main constituent of alluvial deposits resulting from erosion of sedimentary rocks that outcrop in the

reliefs surrounding the SPGS. Ca-HCO_3 waters are hosted both in the shallow (HU3) and deep (HU1) aquifers, but they are more common in the first than in the second one, as they represent the 80% of the samples coming from the shallow aquifer and the 61% of the samples proceeding from the deep aquifer.

The Na-HCO_3 waters have salinity somewhat higher, on average, than the previous chemical type. It is a relatively frequent chemical type in the study area, being represented by 10 samples. The origin of these waters is due to freshening, that is re-circulation of Ca-HCO_3 groundwaters in aquifers previously flooded by seawater and/or brackish water. Also, the Na-HCO_3 waters are hosted both in the shallow and deep aquifers and are more frequent in the first than in the second one, as they represent the 15% of the samples coming from the shallow aquifer and the 10% of the samples proceeding from the deep aquifer.

Most of the Cl waters (14 samples) belong to the Na-Cl chemical type. These are water with a very variable salinity, from 22 to 80 meq/L, generally higher than that of Ca-HCO_3 and Na-HCO_3 waters, but still below the TIS of mean seawater, 1210 meq/L. They are typically of aquifers located near the coast affected by seawater intrusion within the sediments of the alluvial plain. This intrusion can take place directly (salt wedge) or through inflow of seawater and/or brackish water along the riverbeds and their subsequent infiltration into the surrounding aquifers, hosted in the alluvial deposits. The process may be favoured by intense pumping from wells located near riverbeds. Also, the Na-Cl waters are hosted both in the shallow and deep aquifers, but they are more frequent in the second than in the first one, as they represent the 3% of the samples coming from the shallow aquifer and the 27% of the samples proceeding from the deep aquifer suggesting that the most affected aquifer is the deep one.

The two samples ascribable to the Ca-Cl type have SIT of 33-49 meq/L. This is a chemical composition generated by ion exchange consequent to seawater intrusion.

At the end, the complete conceptualisation of the Sibari Plain was able to explain groundwater salinity variations and to support a detailed long-lasting numerical simulation of quality and

quantity variations. It could be considered a reliable tool to support groundwater management, preventing salinization and, at the end, integrating in the future the hydrogeological model with geotechnical routines, preventing excessive subsidence effects for fluid extraction.

Acknowledgement

The authors are particularly grateful to Dr. Luigi Marini for his precious support and advice. This paper is sponsored by PON (Operational National Plan) 2007–13 from MIUR (Italian Research Ministry of Research) Project AMICUS (Resp. Prof.sa Rosanna De Rosa; ID: PON01_ 02818).

References

Adani, M., Dobricic S., Pinardi, N., 2011 Quality Assessment of a 1985–2007 Mediterranean Sea reanalysis. American Meteorological Society, 569-589

Alpert, P., Krichak, S…O, Shafir, H, Haim, D., Osandinsky, I., 2008. Climatic trends to extremes employing regional modeling and statistical interpretation over the E. Mediterranean. Global and Planetary Change 63, 163–170. https://doi:10.1016/j.gloplacha.2008.03.003

Amodio-Morelli, L., Bonardi, G., Colonna, V., Dietrich, D., Giunta, G., Ippolito, F., Liguori, V., Lorenzoni, S., Paglionico, A., Perrone, V., Piccarreta, G., Russo, M., Scandone, P., Zanettin-Lorenzoni, E., and Zuppetta, A. (1976). L'arco Calabro-Peloritano nell'orogene appenninico Maghrebide (The Calabrian-Peloritan Arc in the Apennine-Maghrebide orogen). Memorie della Societ`a Geologica Italiana 17, 1–60

Anderson, M.P., Woessner, W.W., 1992. Applied groundwater modeling: Simulation of flow and advective transport, Academic Press, San Diego, CA.

Apollaro, C., Dotsika, E., Marini, L., Barca, D., Bloise, A., De Rosa, R., Doveri, M., Lelli, M., Muto, F., 2012. Chemical and isotopic characterization of the thermo mineral water of Terme Sibarite springs (Northern Calabria, Italy). Geochem. J. 46, 117–129.

Apollaro, C., Vespasiano, G., De Rosa, R., Marini L., 2015. Use of mean residence time and flowrate of thermal waters to evaluate the volume of reservoir water contributing to the natural discharge and the related geothermal reservoir volume. Application to Northern Thailand hot springs. Geothermics 58, 62–74

Apollaro, C., Vespasiano, G., Muto, F., De Rosa, R., Barca D., Marini L., 2016. Use of mean residence time of water, flowrate, and equilibrium temperature indicated by water

geothermometers to rank geothermal resources. Application to the thermal water circuits of Northern Calabria. Journal of Volcanology and Geothermal Research 328, 147-158.

Apollaro C., Buccianti A., Vespasiano G., Vardè M., Fuoco I., Barca D., Bloise A., Miriello D., Cofone F., Servidio A., De Rosa R. (2019). Comparative geochemical study between the tap waters and the bottled mineral waters in Calabria (southern Italy) by compositional data analysis (CoDA) developments. Applied Geochemistry. 107, 19–33. https://doi.org/10.1016/j.apgeochem.2019.05.011

Appelo, C.A.J., 1994. Cation and proton exchange, pH variations, and carbonate reactions in a freshening aquifer. Water Resources Research 30, 2793-2805.

Appelo, C.A.J., Postma, D., 1996. Geochemistry, groundwater and pollution, A.A. Balkema, Rotterdam.

Appelo, C.A.J.., 1996. Multicomponent ion exchange and chromatography in natural systems, in: Lichtner, P.C., Steefel, C.I., Oelkers, H.E. (Eds.), Reactive Transport in Porous Media, Reviews in Mineralogy 34, pp. 193-227.

Archivio nazionale delle indagini nel sottosuolo L.464/84. ISPRA. http://sgi.isprambiente.it/GMV2/index.html.

Barone, M., Dominici, R., Muto, F., Critelli, S., 2008. Detrital modes in a late Miocene wedge-top basin, northeastern Calabria, Italy: Compositional record of wedge-top partitioning. Journal of Sedimentary Research 78(10), 693-711.

Bellotti, P., Caputo C., Dell'Aglio, P.L., Davoli, L., Ferrari, K., 2009. Insediamenti urbani in un paesaggio in evoluzione: interazione uomo-ambiente nella Piana di Sibari (Calabria ionica). Il Quaternario Italian Journal of Quaternary Sciences 22(1), 61-72.

Bellotti, P., Caputo, C., Davoli, L., Evangelista, S., Pugliese, F., 2003. Sedimentological and morphological evolution of the Crati river delta (Calabria Italy). Suppl. Geogr. Fis. e Din. Quarter. 6, 25-32.

Bernasconi, M.P., Stanley, J.D., Caruso, C., 2010. Sybaris–Thuri–Copia Deltaic Settings in Calabria, Italy:Molluscs, Associated Biogenic Components, and Ecobiostratigraphy Applied to Archaeology. Journal of Coastal Research 26 (2), 377-390.

Betancur, V.T., Palacio, T.C.A., Escobar, M.J.F. 2012. Conceptual Models in Hydrogeology, Methodology and Results. Hydrogeology. A global perspective. Gholam A. Kazemi (Ed.)

Bonardi, G., Amore, F.O., Ciampo, G., De Capoa, P., Miconnet, P., Perrone, V., 1988. Il Complesso Liguride Auct.: stato delle conoscenze e problemi aperti sulla sua evoluzione pre-appenninica ed i suoi rapporti con l'Arco Calabro. Mem. Soc. Geol. Ital. 41, 17-35.

Boughriba, M., Jilali, A., 2018. Climate change and modeling of an unconfined aquifer: the Triffa plain, Morocco. Environment, Development and Sustainability. 20 (5), 2009- 2026.

Caruso, C., Ceravolo, R., Cianflone, G., Dominici, R., Sonnino, M., 2013. Sedimentology and ichnology of Plio-Pleistocene marine to continental deposits in Broglio (Trebisacce, northern ionian Calabria, Italy). Journ. Med. Earth Sc. Spec. Issue, 21-24.

Caruso, C., Natoli, D., Sonnino, M., 2011. Sedimentology and ichnology of the lower part of the Saraceno Formation (Cretaceous? Miocene?) (northern Ionian Calabria). Rendiconti Online Soc. Geol. Ital. 17, 31.

Casmez (Cassa Speciale per il Mezzogiorno), 1967-1969. Carta Geologica della Calabria 1:25000. Foglio 229 I NO, NE, SO, SE; Foglio 230 I NO, SO; IV NO, NE, SO, SE. Poligrafica & Cartevalori, Ercolano, Napoli.

Casmez (Cassa Speciale per il Mezzogiorno), 1987. Progetto Speciale 26. CMP.

Celico, P., 1988. Prospezioni idrogeologiche, Vol. II, Liguori Editore, Napoli.

Cello, G., Tortorici, L., Turco, E., and Guerra, I. (1981). Profili profondi in Calabria settentrionale. Boll. Soc. Geol. It. 109, 423-431.

Changming, L., Jingjie, Y., Kendy, E., 2001. Groundwater exploitation and its impact on the environment in the North China Plain. Water International 26 (2), 265-272.

Cherubini, C., Cotecchia, V., Pagliarulo, R., 2000. Subsidence in the Sybaris Plain (Italy), in: Carbognin, L., Gambolati, G., Johnson, A.I. (Eds.), Land Subsidencee1. Proceedings of the 6th International Symposium on Land Subsidence, Ravenna, pp. 3-15.

Cianflone, G., Cavuoto, G., Punzo, M., Dominici, R., Sonnino, M., Di Fiore, V., Pelosi, N., Tarallo, D., Lirer, F., Marsella, E., Critelli S., De Rosa R., 2018. Late quaternary stratigraphic setting of the Sibari Plain (southern Italy): Hydrogeological implications. Marine and Petroleum Geology 97, 422–436.

Cianflone, G., Dominici, R., Viscomi, A., 2015a. Potential recharge estimation of the Sibari Plain aquifers (southern Italy) through a new GIS procedure. Geographia Technica 10 (1), 8-18.

Cianflone, G., Tolomei C., Brunori, C.A., Dominici R., 2015c. Study of the ground subsidences in the Sibari Plain (Southern Italy) detected by InSAR data analysis. Rendiconti online della Società Geologica Italiana 33, 24-27.

Cianflone, G., Tolomei, C., Brunori, C.A., Dominici, R., 2015b. InSAR time series analysis of natural and anthropogenic coastal plain subsidence: the case of Sibari (Southern Italy). Remote Sensing 7, 16004–16023.

Cinti, F.R., Alfonsi, L., D'Alessio, A., Marino, S., Brunori C.A., 2015. Faulting and Ancient Earthquakes at Sybaris Archaeological Site, Ionian Calabria, Southern Italy. Seismological Research Letters 86 (1), 245-254.

Civita, M., 2005. Idrogeologia applicata ed ambientale, Casa Editrice Ambrosiana, Milano.

Comerci, V., Blumetti, A.M., Di Manna, P., Fiorenza, D., Guerrieri, L., Lucarini, M., Serva, L., Vittori E., 2013. ITHACA Project and Capable Faults in the Po Plain (Northern Italy). Ingegneria Sismica Spec. Issue 1-2-January-June 2013, 36-50.

Cotecchia, V., D'Ecclesiis, G., Polemio, M., 1990. Studio geologico e idrogeologico dei monti di Maratea: Geologia Applicata e Idrogeologia XXV, 139-179.

Critelli, T., Vespasiano, G., Apollaro, C., Muto, F., Marini, L., De Rosa, R., 2015. Hydrogeochemical study of an ophiolitic aquifer: a case study of Lago (Southern Italy, Calabria). Environmental Earth Sciences 74, 533-543

Cucci, L., 2004. Raised marine terraces in the Northern Calabrian Arc (Southern Italy): a ~600 Ka-long geological record of regional uplift. Annals of Geophysics 47, 1391-1406.

Cucci, L., Cinti, F.R., 1998. Regional uplift and local tectonic deformation recorded by the Quaternary marine terraces on the Ionian coast of northern Calabria (southern Italy). Tectonophysics 292, 67-83.

D'Alessandro, A., Ekdale, A.A., Sonnino, M., 1986. Sedimentologic significance of turbidite ichnofacies in the Saraceno Formation (Eocene), Southern Italy. Jour. Sedim. Petrol. 56, 294-306.

Datta, P.S., Deb, D.L., Tyagi S.K., 1997. Assessment of groundwater contamination from fertilizers in the Delhi area based on ^{18}O, NO_3 and K^+ composition. Journal of Contaminant Hydrology. 27, 249-262

Davis, S.N., 1969. Porosity and permeabiliy of natural materials. Flow through porous media, De Wiest R.J.M. (Ed.), Academic Press, New York

De Blasio, I., Lima, A., Perrone, V., Russo, M., 1978. Studio petrografico e biostratigrafico di una sezione della Formazione del Saraceno nell'area tipo (Calabria nord-orientale). Riv. It. Paleont. 84, 947-972.

De Montety, V., Radakovitch, O., Vallet-Coulomb, C., Blavoux, B., Hermitte, D., Valles, V., 2008. Origin of groundwater salinity and hydrogeochemical processes in a confined coastal aquifer: case of the Rhone delta (Southern France). Applied Geochemistry 23 (8), 2337–2349.

Di Staso, A., Giardino, S., 2002. New integrate biostratigraphic data about the Saraceno formation (North-Calabrian Unit; Southern Apennines). Boll. Soc. Geol. It. Spec. Issue 1, 517-526.

Domenico, P.A., 1972. Concepts and models in groundwater hydrology, McGraw-Hill, New York.

Ferranti, L., Pagliarulo, R., Antonioli, F., Randisi, A., 2011. Punishment for the sinner: Holocene episodic subsidence and steady tectonic motion at ancient Sybaris (Calabria, southern Italy). Quaternary International 232, 56-70.

Ferranti, L., Santoro, E., Mazzella, M.E., Monaco, C., Morelli, D., 2009. Active transpression in the northern Calabria Apennines, southern Italy. Tectonophysics 476, 226–251.

Finetti, I., Lentini, F., Carbone, C., Catalano, S., and Del Ben, A. (1996). Il sistema Apennino meridionale-Arco Calabro-Sicilia nel Mediterraneo centrale: sudio geologico-geofisico. Boll. Soc. Geol. It. 115, 529-559

Fraser, G.S., Davis, J.M., 1998. Hydrogeologic models of sedimentary aquifers. SEPM Concepts in Hydrogeology and Environmental Geology 1, 188 pp.

Galloway, W.E., Sharpe, J.M., 1998a. Hydrogeology and characterization of fluvial aquifers systems. In Fraser, G.S. and Davis, J.M. eds.: Hydrogeologic models of sedimentary aquifers. SEPM Concepts in Hydrogeology and Environmental Geology 1, 91-106.

Galloway, W.E., Sharpe, J.M., 1998b. Characterizing aquifers heterogeneity within terrigenous clastic depositional systems. In Fraser, G.S. and Davis, J.M. eds.: Hydrogeologic models of sedimentary aquifers. SEPM Concepts in Hydrogeology and Environmental Geology 1, 85-90.

Geoportale Nazionale (GN), Ministero dell'Ambiente. Modello digitale del terreno - 20 metri. http://wms.pcn.minambiente.it/wcs/dtm_20m.

Ghisetti, F., Vezzani, L., 1983. Deformazioni pellicolari mioceniche e plioceniche nei domini strutturali esterni dell'Appennino centro-meridionale (Maiella ed Arco Morrone-Gran Sasso). Mem. Soc. Geol. It. 26, 563-577.

Gibelin, A.L., Déqué, M., 2003. Anthropogenic climate change over the Mediterranean region simulated by a global variable resolution model. Climate Dynamics 20, 327–339.

Giorgi, F., Lionello, P., 2008. Climate change projections for the Mediterranean region. Global and Planetary Change 63, 90–104.

Goubanova, K., Li, L., 2007. Extremes in temperature and precipitation around the Mediterranean basin in an ensemble of future climate scenario simulations. Global and Planetary Change 57, 27–42.

Grauel, A..L, Nernasconi, S.M., 2010. Core-top calibration of $\delta^{18}O$ and $\delta\ ^{13}C$ of G. ruber (white) and U. mediterranea along the southern Adriatic coast of Italy. Marine Micropaleontology 77, 175-186.

Guerricchio, A., Melidoro, G., 1975. Ricerche di geologia applicata all'Archeologia dell'antica città di Sibari sepolta. Geologia Applicata e Idrogeologia X, 107-128.

Guerricchio, A., Melidoro, G., Tazioli, G.S., 1976. Lineamenti idrogeologici e subsidenza dei terreni olocenici della Piana di Sibari, in: Rivista Sviluppo 9. Cassa di Risparmio di Calabria e Lucania, Cosenza

Guerricchio, A., Ronconi, M.L., 1997. Osservazioni geomorfologiche nella piana di Sibari e variazioni delle linee di costa storiche nella zona degli scavi archeologici. I Quaderni dell'IRFEA 12, 5-31.

Guo, W., Langevin, C..D, 2002. User's Guide to SEAWAT: A Computer Program for Simulation of Three-Dimensional Variable-Density Ground-Water Flow, U.S. Geological Survey Open-File Report 01-4340.

Haruyama, S., 2016. Introduction-overview of natural disasters and coastal landforms, in: Natural Disaster and Coastal Geomorphology, pp. 1-13. 1

Hofman, B., 2002. The Sedimentation History of the Sybaris Plain, University of Groningen, Mediterranean Archaeology Report, 28 p.

InTech, 7, 203-222.Bocanegra, E. M., Polemio, M., Massone, H. E., Dragone, V., Limoni, P. P., Farenga, M., 2007. Indicators and quality classification applied to groundwater management in coastal aquifers: Mar del Plata (Argentina) and Apulia (Italy) case studies, in: Sanford, W., Langevin, C., Polemio, M., Povinec, P. (Eds.), A new focus on groundwater-seawater interactions, Volume 312, IAHS, pp. 201-211.

ISPRA public geodatabase of borehole data on http://portalesgi.isprambiente.it/it/categorie-db/sondaggi

ISPRA, 2009. Carta Geologica d'Italia alla scala 1:50.000. Foglio 535, Trebisacce.

ISPRA, 2010. Carta Geologica d'Italia alla scala 1:50.000. Foglio 543, Cassano allo Ionio.

Jalali M., 2007. Site-specific potassium application based on the fertilizer potassium availability index of soil. Precision Agric, 8, 199–211

Johnson, A.I., 1967. Specific Yield - Compilation of specific yields for various materials. U.S. Geological Survey Water-Supply Paper 1662-D

Jumikis, A.R., 1962. Soil Mechanics. D. Van Norstrand Book Company, New York

Langevin, C., Sanford, W., Polemio, M., Povinec, P., 2007. Background and summary a new focus on groundwater-seawater interactions, in: Sanford, W., Langevin, C., Polemio, M., Povinec, P. (Eds.), New focus on groundwater-seawater interactions, Vol. 312. IAHS, p. 3-10.

Langevin, C.D., 2003. Simulation of Submarine Ground Water Discharge to a Marine Estuary: Biscayne Bay, Florida. Ground Water 41 (6), 758–771.

Langmuir, D., 1996. Aqueous environmental geochemistry. Prentice-Hall, Inc. Upper Saddle River, NJ. pp 602.

Lanzafame, G., Tortorici, L., 1981. La tettonica recente del Fiume Crati (Calabria). Geografia Fisica e Dinamica Quaternaria 4, 11–21.

Longinelli, A., Selmo, E., 2003. Isotopic composition of precipitation in Italy: a first overall map. J. Hydrol. 270, 75-88.

Marini, L., 2006. Geological Sequestration of Carbon Dioxide - Thermodynamics, Kinetics, and Reaction Path Modeling. Developments in Geochemistry 11, 453 pp.

Martin, P.J., Frind, E.O., 1998. Modeling a complex multi-aquifer system: The Waterloo Moraine. Groundwater 36(4), 679-690.

Matiatos, I., Paraskevopoulou, V., Lazogiannis, K., Botsou, F., Dassenakis, M., Ghionis, G., Alexopoulos, J.D., Poulos, S.E., 2018. Surface–ground water interactions and hydrogeochemical evolution in a fluvio-deltaic setting: The case study of the Pinios River delta. Journal of Hydrology. 561, 236 – 249.

McDonald, M.G., Harbaugh, A.W., 1988. A modular three-dimensional finite-difference ground-water flow model. Techniques of Water-Resources Investigations of the United States Geological Survey 6.

Messina, A., Russo, S., Borghi, A., Colonna, V., Compagnoni, R., Caggianelli, A., Fornelli, A., and Piccarreta, G. (1994). Il Massiccio della Sila, Settore settentrionale dell'Arco Calabro-Peloritano (The Sila Massif, northern sector of the Calabrian-Peloritan Arc). Boll. Soc. Geol. It., 113, 539–586.

Molin, P., Pazzaglia, F.J., Dramis, F., 2004. Geomorphic expression of active tectonics in a rapidly-deforming forearc, Sila Massif, Calabria, Southern Italy. American Journal of Science 304, 559-589.

Nollet, L.M.L., De Gelder, L.S.P., 2007. Handbook of Water Analysis, CRC Press, 944 pp.

Nordstrom, D.K., 2000. Advances in the hydrogeochemistry and microbiology of acid mine waters. Int. Geol. Rev. 42, 499-515.

Nordstrom, D.K., Plummer, L.N., Wigley, T.M.L., Wolery, T.J., Ball, J.W., Jenne, E.A., Basset, R.L., Crerar, D.A., Florence, T.M., Fritz, B., Hoffman, M., Holdren, G.R.Jr., Lafon, G.M., Mattigod, S.V., McDuff, R.E., Morel, F., Reddy, M.M., Sposito, G., Thrailkill, J., 1979. A comparison of computerized chemical models for equilibrium calculations in aqueous systems, in Jenne E.A. (Ed.), Chemical Modeling in Aqueous Systems. ACS Symposium Series 93, 857-892.

Pagliarulo, R., 2006. Coastal changes and the environmental evolution of the archaeological site of Sybaris (Southern Italy). Geografia Fisica e Dinamica Quaternaria 29, 51-59.

Perri, F., Dominici, R., Critelli, S., 2015. Stratigraphy, composition and provenance of argillaceous marls from the Calcare di Base Formation, Rossano Basin (northeastern Calabria). Geological Magazine 152(2), 193-209.

Petrucci, O., Polemio, M., 2007. Flood risk mitigation and anthropogenic modifications of a coastal plain in southern Italy: combined effects over the past 150 years. Natural Hazards and Earth System Sciences 7 (3), 361-373.

Pierre, C., 1999. The oxygen and carbon isotope distribution in the Mediterranean water masses. Marine Geology 153, 41-55.

Pisinaras, V., Petalas, C., Tsihrintzia, V.A., Zagana, E., 2007. A groundwater flow model for water resources management in the Ismarida plain, North Greece. Environmental Modeling and Assessment 12, 75-89.

Polemio, M., 2016. Monitoring and Management of Karstic Coastal Groundwater in a Changing Environment (Southern Italy): A Review of a Regional Experience. Water 8, 1-16. https://doi:10.3390/w8040148 (2016).

Polemio, M., Casarano, D., 2004. Rainfall and drought in Southern Italy (1821–2001). The basis of civilization water science?. IAHS publ. 286, 217-227.

Polemio, M., Casarano, D., Dragone, V., 2004. Trend termopluviometrici, siccità e disponibilità di acque sotterranee, in: Atti della Giornata di Studio: Metodi Statistici e Matematici per l'Analisi delle Serie Idrologiche, Napoli, pp. 123-132.

Polemio, M., Dragone, V., Romanazzi, A.. 2013, La risorsa idrica. Sfruttamento, depauperamento dei serbatoi sotterranei e utilizzo razionale nel caso della Calabria, in: Dramis, F., Mottana, A. (Eds.), L'acqua in Calabria: risorsa o problema?. Aracne, Roma, pp. 2-29.

Polemio, M., Lonigro, T., 2015. Trends in climate, short-duration rainfall, and damaging hydrogeological events (Apulia, Southern Italy): Natural Hazards 75 (1), 515-540.

Polemio, M., Luise, G., 2007. Conceptual and numerical model of groundwater flow for a coastal plain (Piana di Sibari, Southern Italy), in: Ribeiro, L., Chambel, A., and Condesso de Melo, M. T. (Eds.), Groundwater and Ecosystems, p. 10.

Polemio, M., Petrucci, O., Gatto, L., 2004. Suscettività alla siccità in Calabria ed effetti sulle acque sotterranee. Atti dei Convegni lincei 204, 245-250.

Ragab, R., Prudhomme, C., 2002. Climate change and water resources management in arid and semi-arid regions: Prospective and challenges for the 21st century. Biosystems Engineering, 81 (1), 3-34.

Rehm, B.W., Groenewold, G.H., Morin, K.A., 1980. Hydraulic properties of coal and related materials, Northern Great Plains. Ground Water 18(6), 551-561.

Sabato, L., Tropeano, M., 2008. The Holocene coastal alluvial fan of the Saraceno Fiumara (Calabria, Southern Italy): highstand filling of an incised valley, in: Amorosi, A., Haq, B.U., Sabato, L. (Eds.), Advance in Application of Sequence Stratigraphy in Italy. GeoActa S.P. 1, 15-27.

Sanford, W., Langevin, C., Polemio, M., Povinec, P., 2007. A new focus on groundwater-seawater interactions. IAHS 312, 3-10.

Santoro, E., Mazzella, M.E., Ferranti, L., Randisi, A., Napolitano, E., Rittner, S., and Radtke, U., 2009. Raised coastal terraces along the Ionian Sea coast of northern Calabria, Italy, suggest space and time variability of tectonic uplift rates. Quaternary International 206, 78-101.

Sanz D., Gómez-Alday J.J., Castaño S., Moratalla A., De las Heras J., Martínez-Alfaro P.E., 2009. Hydrostratigraphic framework and hydrogeological behaviour of the Mancha Oriental System (SE Spain). Hydrogeology Journal 17, 1375–1391.

Schmidt, G.A., Bigg, G.R., Rohling, E.J., 1999. Global Seawater Oxygen-18 Database - v1.21 http://data.giss.nasa.gov/o18data/

Selli, R., 1962. Il Paleogene nel quadro della geologia dell'Italia centro-meridionale. Mem. Soc.Geol. It. 3, 737-789.

Shamrukh, M., Corapcioglu, M. Y., and Hassona, A. A., 2001. Modeling the effect of chemical fertilizers on Groundwater quality in the Nile Valley Aquifer, Egypt. Groundwater, 39, 59-67.

Skowron, P., Skowrońskaa,M., Bronowicka-Mielniczukb, U., Filipeka, T., Igrasc, J., Kowalczyk-Juśkod, A., Krzepiłkoe A., 2018. Anthropogenic sources of potassium in surface water: The case study of the Bystrzyca river catchment, Poland. Agriculture, Ecosystems and Environment. 265 , 454–460.

Sonnino, M., 1984. Un example d'évolution de dépôts de plateforme à dépôts de bassin: la Formation du Saraceno (Eocène moyen-sup., Italie du Sud). 5ème Congr. Europ. Sédim., Marseille, Abstr., 479-480.

Spina, V., Tondi, E., and Mazzoli, S., 2011. Complex basin development in a wrench-dominated back-arc area:Tectonic evolution of the Crati Basin, Calabria, Italy. Journal of Geodynamics 51, 90–109.

Stanley, J.D., Bernasconi, M.P., 2009. Sybaris-Thuri-Copia trilogy: three delta coastal sites become land-locked. Méditerranée 112, 75–86.

Stenni, B., Nichetto, P., Bregant, D., Scarazzato, P., Longinelli, A., 1995. The $\delta^{18}O$ signal of the northward flow of Mediterranean waters in the Adriatic Sea. Oceanologica Acta 18, 319-328.

Tazioli, G.S., 1986. Indagini idrogeologiche volte allo sfruttamento delle risorse idriche sotterranee. Tecniche per la difesa dell'inquinamento, VII Conferenza di Aggiornamento, Cosenza

Teatini, P., Ferronato, M., Gambolati, G., Gonella, M. (2006). Groundwater pumping and land subsidence in the Emilia-Romagna coastland, Italy: Modeling the past occurrence and the future trend. Water Resources Research, 42 (1), W01406. https://doi.org/10.1029/2005WR004242

Tonani, F., Nagao, K., Moore, J., Natale, G., Sperry, T., 1998. Water and gas geochemistry of the Cove-Fort Sulphurdale geothermal system, in: Proceedings of 23rd Workshop on Geothermal Reservoir Engineering. Stanford University, Stanford, California, January 26-28.

Torricelli, S., Amore, M.R., 2003. Dinoflagellate cyst and calcareous nannofossils from the Upper Cretaceous Saraceno Formation (Calabria, Italy): implications about the history of the Liguride Complex. Riv. It. Paleont. Strat. 109, 499-516.

Tsimplis, M.N., Marcos, M., Somot S., 2008. 21st century Mediterranean Sea level rise: Steric and atmospheric pressure contributions from a regional model. Global and Planetary Change 63, 105–111.

Vardè, M., Servidio, A., Vespasiano, G., Pasti, L., Cavazzini, A., Di Traglia, M., Rosselli, A., Cofone, F., Apollaro, C., Cairns, W.R.L., Scalabrin, E., De Rosa, R., Procopio, A., 2019. Ultra-trace determination of total mercury in Italian bottled waters. Chemosphere 219, 896–913. https://doi.org/10.1016/j.chemosphere.2018.12.020.

Vespasiano, G., Apollaro C., 2016c. Preliminary geochemical characterization of a carbonate aquifer: the case of Pollino massif (Calabria, South Italy). Rend. Online. Soc. Geol. It., 38, 109-112

Vespasiano, G., Apollaro, C., De Rosa, R., Muto, F., Larosa, S., Fiebig, J., Mulch, A., Marini, L., 2015c. The Small Spring Method (SSM) for the definition of stable isotope - elevation relationships in Northern Calabria (Southern Italy). Applied Geochemistry 63, 333-346.

Vespasiano, G., Apollaro, C., Marini, L., Dominici, R., Cianflone, G., Romanazzi, A., Polemio, M., De Rosa R., 2015a. Hydrogeological and isotopic study of the multi-aquifer system of the Sibari Plain (Calabria, Southern Italy). Rend. Online Soc. Geol. It. 39, 134-137

Vespasiano, G., Apollaro, C., Muto, F., De Rosa, R., Critelli, T., 2015b. Preliminary geochemical and geological characterization of the thermal site of Spezzano Albanese (Calabria, South Italy). Rend. Online Soc. Geol. It. - Vol. 33, 108-110

Vespasiano, G., Apollaro, C., Muto, F., De Rosa, R., Dotsika, E., Marini, L., 2015d. Preliminary geochemical characterization of the warm waters of the Grotta delle Ninfe near Cerchiara di Calabria (South Italy). Rend. Online. Soc. Geol. It. 39, 130-133

Vespasiano, G., Apollaro, C., Muto, F., Dotsika, E., De Rosa, R., Marini, L., 2014. Chemical and isotopic characteristics of the warm and cold waters of the Luigiane Spa near Guardia Piemontese (Calabria, Italy) in a complex faulted geological framework. Applied Geochemistry 41, 73-88.

Vespasiano, G., Cianflone, G., Cannata, C.B., Apollaro, C., Dominici, R., De Rosa R., 2016a. Analysis of groundwater pollution in the Sant'Eufemia Plain (Calabria – South Italy). Italian Journal of Engineering Geology and Environment 16 (2), 5-15.

Vespasiano, G., Marini, L., Apollaro, C., De Rosa, R., 2016b. Preliminary geochemical characterization of the thermal waters of Caronte SPA springs (Calabria, South Italy). Rend. Online Soc. Geol. It. 39, 138-141

Vezzani, L., 1968. Studio stratigrafico della Formazione delle Crete Nere (Aptiano-Albiano) al confine calabrolucano. Atti Ac. Gioenia Se. Nat. Catania 20, 189-222.

ViDEPI, Visibilità Dati Esplorazione Petrolifera in Italia. http://unmig.sviluppoeconomico.gov.it/videpi/kml/webgis.asp

Wolery, T.W., Jarek R.L., 2003. Software user's manual. EQ3/6, Version 8.0. Sandia National Laboratories – U.S. Dept. of Energy Report.

Zuffianò, L. E., Basso, A., Casarano, D., Dragone, V., Limoni, P. P., Romanazzi, A., Santaloia, F., Polemio, M., 2016. Coastal hydrogeological system of Mar Piccolo (Taranto, Italy). Environmental Science and Pollution Research 23 (13), 12502-12514.

Table captions

Table 1a. Field parameters and concentrations of major chemical components and selected minor components in the SPGS wells. (d.l. = detection limit; n.d. = not detected; n.a. = not available).

Table 1b. Field parameters and concentrations of major chemical components and selected minor components in the SPGS wells (d.l. = detection limit; n.d. = not detected; n.a. = not available).

Table 2. Statistical indices of pH, temperature (T), and electric conductivity (EC), and Eh of SPGS groundwaters.

Table 3. The distribution of chemical type in the HU3 and HU1 aquifers .

Table 4. Variation of the aqueous solution (average seawater) chemistry during ion exchange upon seawater intrusion. Xi represents the moles of cation exchanger added to 1 kg of average seawater.

Table 5. Variation of the aqueous solution (average groundwater) chemistry during ion exchange upon groundwater inflow into an aquifer previously affected by seawater intrusion. Xi represents the moles of cation exchanger added to 1 kg of average groundwater.

Table 6. Analytical ™^{18}O and ™^{2}H values of seawater-contaminated SPGS groundwaters, computed $\delta^{18}O^*$ and $\delta^{2}H^*$ values of corresponding pure groundwaters, and average infiltration altitudes, Hi, calculated from the $\delta^{18}O^*$ and $\delta^{2}H^*$ values. In bold samples representative of the deep aquifer.

Table 7 – Calibration of the hydraulic conductivity for each hydrogeological unit.

Figure captions

Figure 1 – (a) Simplified geological map of the study area. Fault traces are derived from Ithaca database (Comerci et al., 2013) while Sybaris Fault Zone (SZF) is from Cinti et al. (2015). (b) Deep seismic profile, modified from Cello et al. (1981), showing the thin Calabrid units overlapping the Southern Apennine units.

Figure 2 – Location of alluvial fans and sampled wells.

Figure 3 - Hydrostratigraphic cross-sections of the Saraceno alluvial fan (X-X'), the Satanasso alluvial fan (Y-Y') and the Crati Delta area (Z-Z') the electrical resistivity profile crossing the Raganello alluvial fan (K-K', redrawn from Camez, 1987).

Figure 4 - a) Shallow aquifer HU3 thickness map (m). b) Depth (m asl) of the HU2 aquitard bottom.

Figure 5. Triangular plots of (a) major anions and (b) major cations for the SPGS groundwaters.

Figure 6 - Correlation diagram of $Ca + Mg + HCO_3 + SO_4$ vs. $Na + K + Cl$ for the SPGS groundwaters.

Figure 7. (a) Variation of the concentrations of major dissolved constituents and (b) Moles of solid phases precipitated as a function of the moles of cation exchanger added to 1 kg of average seawater.

Figure 8. (a) Variation of the concentrations of major dissolved constituents and (b) Mole of calcite precipitated as a function of the moles of cation exchanger added to 1 kg of average groundwater.

Figure 9. Correlation diagrams of Na+K vs. Ca+Mg showing the results of geochemical modeling for ion exchange processes triggered by seawater intrusion and freshening.

Figure 10. Triangular plots of (a) major cations and (b) major anions, both prepared starting from concentrations in equivalent units, showing the effects of ion exchange processes accompanying seawater intrusion and freshening.

Figure 11 - Log-log diagrams of Na vs. Cl and Ca vs. Cl for the SPGS aquifers (HU1 and HU3) also showing average seawater and the mixing lines between average seawater and the groundwater endmember (samples P56 and P47 - HU1 aquifer; P12 and P15 – HU3 aquifer). The arrow "ion exchange" refers to the effects expected for seawater intrusion.

Figure 12. Log-log diagrams of Mg vs. Cl and K vs. Cl for the SPGS aquifers, also showing the mixing lines between average seawater and groundwater.

Figure 13 - Binary diagrams $\delta^{18}O$ vs. δD.

Figure 14 – Conceptual model and hydrogeological complex.

Figure 15 – 3d view of DTM and of the SPGS hydrogeological conceptualisation, using hydrogeological complexes, and grid discretisation (“fiumare” describes geometry and location of riverbeds).

Figure 16 - 3d view of shallow groundwater salinity: A) steady state; B) expected in 2020.

Figure 17 - W-E section: lateral intrusion and up-coning effect under the Sybaris archaeological site (Ionian Sea on the right or Eastern side of the figure)

Hydrostratigraphy related to Quaternary coastal plain evolution.

Groundwaters are affected by salinization and freshening phenomena.

Numerical simulations show groundwater qualitative and quantitative degradation.